Protostellar Outflows

John Bally

Department of Astrophysical and Planetary Sciences, University of Colorado, Boulder, Colorado 80389; email: john.bally@colorado.edu

Annu. Rev. Astron. Astrophys. 2016. 54:491–528

The *Annual Review of Astronomy and Astrophysics* is online at astro.annualreviews.org

This article's doi: 10.1146/annurev-astro-081915-023341

Keywords

star formation, bipolar molecular outflows, Herbig-Haro objects, protostellar jets, molecular hydrogen objects, feedback, self-regulation of star formation

Abstract

Outflows from accreting, rotating, and magnetized systems are ubiquitous. Protostellar outflows can be observed from radio to X-ray wavelengths in the continuum and a multitude of spectral lines that probe a wide range of physical conditions, chemical phases, radial velocities, and proper motions. Wide-field visual and near-IR data, mid-IR observations from space, and aperture synthesis with centimeter- and millimeterwave interferometers are revolutionizing outflow studies. Many outflows originate in multiple systems and clusters. Although most flows are bipolar and some contain highly collimated jets, others are wide-angle winds, and a few are nearly isotropic and exhibit explosive behavior. Morphologies and velocity fields indicate variations in ejection velocity, mass-loss rate, and in some cases, flow orientation and degree of collimation. These trends indicate that stellar accretion is episodic and often occurs in a complex dynamical environment. Outflow power increases with source luminosity but decreases with evolutionary stage. The youngest outflows are small and best traced by molecules such as CO, SiO, H_2O, and H_2. Older outflows can grow to parsec scales and are best traced by shock-excited atoms and ions such as hydrogen-recombination lines, [SII], and [OII]. Outflows inject momentum and energy into their surroundings and provide an important mechanism in the self-regulation of star formation. However, momentum injection rates remain uncertain with estimates providing lower bounds.

Contents

1. INTRODUCTION

Accreting astrophysical systems with rotation and magnetic fields tend to exhibit bipolar outflows or collimated jets. Examples include young stellar objects (YSOs), symbiotic stars, post-main-sequence objects such as protoplanetary nebulae, planetary nebulae, some supernovae, accreting neutron stars such as SS433, microquasars, active galactic nuclei, and quasars (Livio 2011). Dimensionless parameters such as the ejecta speed divided by the Kepler speed at the launch point, the degree of collimation, morphology, and variability in mass-loss rate, ejection velocity, ejection direction, and degree of collimation are similar in all classes of accretion-powered outflows. However, there are also significant differences, such as outflow speed, which can range from a few km s^{-1} to over 10^3 km s^{-1} for forming stars, to nearly the speed of light for outflows powered by neutron stars and black holes. There are hundreds of YSO outflows within 1 kpc of the Sun. Spectral lines allow measurements of radial velocities and physical parameters such as density, temperature, and pressure over a wide range of conditions (for a recent review, see Frank et al. 2014). Many outflows are sufficiently close to enable proper motion measurements. Their morphology, kinematics, and physical properties provide fossil records of the mass ejection and, by inference, the mass accretion histories of forming young stars.

A number of apparently unrelated phenomena were discovered in regions where stars have formed recently. These include the emission-line spectra and erratic variability of the "objects of Joy" (Rydgren et al. 1976, p. 307; see also Joy 1945), pre-main-sequence stars with masses less than about 2 $M_\odot$ that came to be known as T Tauri stars. Stars with similar properties but with spectral types ranging from B to F, higher luminosities, and masses around 2 to ~8 $M_\odot$ came to be known as Herbig AeBe stars (Herbig 1960). Herbig (1951) and Haro (1952) discovered small emission-line nebulae in dark clouds with peculiar spectra when compared with HII regions. These Herbig-Haro (HH) objects trace supersonic shock waves. A subset of HH objects are highly collimated jets (Dopita et al. 1982, Mundt & Fried 1983, Reipurth et al. 1986, Reipurth & Bally 2001). A catalog of HH objects is available online (**http://vizier.u-strasbg.fr/viz-bin/VizieR?-source=HH**); for an account of Herbig's contributions to our understanding of star formation, see Reipurth (2016). The first published spectrum of interstellar carbon monoxide (CO) revealed broad line wings with

YSO: young stellar object

Herbig-Haro (HH) object: a shock-excited, visual wavelength nebulosity powered by an outflow from a young star

$\Delta V > 100$ km s^{-1} (Wilson et al. 1970) and indicated a supersonic outflow from the BN/KL region behind the Orion Nebula (Kwan & Scoville 1976, Zuckerman et al. 1976). Following the discoveries of the bipolar outflow from L1551 in Taurus (Snell et al. 1980) and a few other sources, it was recognized that molecular outflows are common in star forming regions (Bally & Lada 1983, Lada 1985, Bachiller 1996, Frank et al. 2014). For a catalog of molecular outflows, see Wu et al. (2004). Thermal and non-thermal radio continuum was found near YSOs too cold to produce significant ionizing radiation (Cohen et al. 1982, Snell & Bally 1986). Maser emission in transitions of OH and H_2O was discovered near YSOs; SiO and CH_3OH masers were found near massive young stellar objects (MYSOs) (Weaver et al. 1965, Cheung et al. 1969, Ball et al. 1970). Near-IR observations led to the discovery of shock-excited H_2 in outflows. A catalog of over 1,000 molecular hydrogen objects (MHOs) has been compiled by Davis et al. (2010). By the late 1980s, these phenomena were recognized to be different manifestations of the supersonic ejection of matter accompanying accretion during star formation and pre-main-sequence stellar evolution.

MYSO: massive young stellar object

Molecular hydrogen object (MHO): shock-excited, near-IR emission from H_2 powered by an outflow from a young star

2. OUTFLOWS FROM YOUNG STELLAR OBJECTS

The morphologies, sizes, and velocities of outflows depend on the specific tracer used and on the luminosity, mass, evolutionary stage, and age of the source YSO; the durations of active accretion and outflow-driving phases; and the properties of the environment into which the flow is moving. The low-J pure rotational transitions of CO have been the most used tracers of molecular outflows. CO is abundant [N(CO) $\sim 10^{-4}$N(H_2)]; its lowest energy levels ($E_u/k = 5.5$, 16.5, and 33 K above ground for the $J = 1$, 2, and 3 rotational states, respectively) are easily populated by collisions with H_2 and He at the typical densities and temperatures of molecular clouds. These CO emission lines are accessible from the ground in the 3-, 1.3-, and 0.85-mm atmospheric windows. However, the higher-J transitions of CO, species such as SiO and H_2O whose abundances can be increased in shocks, and shock-excited H_2 are more selective of the accelerated warm and hot gas in molecular outflows. Grain sputtering in shocks can enhance gas-phase SiO and H_2O abundances by orders of magnitude compared with the surrounding cold cloud (Nisini et al. 2007, 2013; Kristensen et al. 2011). Shocks can also drive endothermic chemical reactions leading to the formation of species not formed in cold gas. Metal hydrides observed in the ISM may owe their origins to shocks (see Gerin et al. 2016 in this volume).

Hundreds of bipolar molecular outflows traced by CO are known (Fukui et al. 1993, Wu et al. 2004). The compilation of 68 molecular outflows by Lada (1985) indicated that their mechanical luminosity scales with the source luminosity and that the momentum in outflows is orders of magnitude larger than that supplied by radiation pressure. Thus, powerful hydrodynamic (HD) or magnetohydrodynamic (MHD) forces are required to accelerate the primary winds responsible for entraining the observed molecules.

Visual and near-IR emission lines in the Balmer, Paschen, and Brackett series of hydrogen; forbidden transitions of [SII], [OI], [OII], [OIII], and [NII]; and the near emission lines of H_2 and [FeII] trace the atomic and ionized components in outflows. Near-IR K-band emission in the rovibrational transition of H_2 trace $\sim$10 to 100 km s^{-1} shocks propagating into molecular gas (MHOs). The *Hubble Space Telescope* (HST) and ground-based adaptive optics provide subarcsecond resolution at visual and near-IR wavelengths. During the past two decades, wide-field imaging at visual and near-IR wavelengths has shown that outflows can be very large. Chains of HH objects with angular sizes of degrees in nearby clouds such as Taurus, Chamaeleon, and Orion indicate that outflows can be many parsecs in extent, with a few exceeding 10 pc (Ogura 1995; Reipurth et al. 1997a; Bally et al. 2006b, 2012a). The radio continuum can trace jets near their sources and, in some outflows, acceleration of relativistic particles that produce synchrotron emission

(Rodríguez-Kamenetzky et al. 2015). X-rays have been detected from a few outflows indicating fast shocks and mega-Kelvin plasmas (Pravdo et al. 2001, 2004; Pravdo & Tsuboi 2005). The *Infrared Space Observatory* (ISO), the *Spitzer Space Observatory* (*Spitzer*), and the *Herschel Space Observatory* (*Herschel*) have extended outflow studies into the mid- and far-IR wavelength regime where extinction is low and most of the luminosity of shocked gas emerges (Maret et al. 2009, Neufeld et al. 2009, van Dishoeck et al. 2011, Kristensen et al. 2012). The submillimeter and far-IR fine-structure lines such as [OI] trace the neutral atomic component (Nisini et al. 2015), and lines such as [CII] and [NII] trace the ionized component. Stratospheric Observatory for Infrared Astronomy (SOFIA) continues studies of mid- and far-IR emission lines. Millimeter- and submillimeter-wavelength interferometers provide arcsecond angular resolution images and data cubes (Arce et al. 2013). Thus, protostellar outflows can be probed using a very wide array of tracers. No tracer is perfect. A complete characterization of the outflow phenomenon requires the observation of many tracers.

Infrared Space Observatory (ISO): mission launched in 1995

Spitzer Space Observatory (Spitzer): mission launched in 2003

Herschel Space Observatory (Herschel): mission launched in 2009

Atacama Large Millimeter Array (ALMA): telescope in Chile

Protostellar outflows are the lowest rung in a ladder of ever-stronger feedback impacts in the self-regulation of star formation. For forming low-mass YSOs isolated from massive stars, outflows may be the dominant source of feedback (Elmegreen & Scalo 2004, Scalo & Elmegreen 2004, De Colle & Raga 2005, Matzner 2007). Combined with the dynamics of multibody systems, feedback may help to determine final stellar masses and the shape of the initial mass function (Reipurth & Mikkola 2012, Nakamura & Li 2014, Guszejnov et al. 2015). Feedback can disrupt the parent clouds and terminate star formation, thereby determining the fraction of a cloud's mass converted into stars, i.e., the star-formation efficiency (Vázquez-Semadeni et al. 2010, Colín et al. 2013). In this review, the phenomenology, physics, and impacts of outflows from young stars are discussed with an emphasis on the developments during the past two decades.

2.1. A Low-Mass Example: HH 46/47

HH 46/47 in an ~8-$M_\odot$ cloud located at a distance of 450 pc is a prototypical mature outflow (van Kempen et al. 2009). At visual wavelengths, the brightest part consists of an [SII] dominated, blue-shifted jet (**Figure 1**) driven by an embedded ~15–30-$L_\odot$ Class I binary YSO toward two bow-shocks (HH 47A and D in **Figure 2**). The λλ6717/6731 Å [SII] doublet requires shock speeds of tens of km s^{-1} to excite. However, the jet exhibits proper motions of ~300 km s^{-1} and radial velocities of approximately −150 km s^{-1} (Hartigan et al. 2011). Thus, [SII] traces weak shocks produced by low-amplitude velocity variations in a fast flow that excites the low-lying, few electronvolt transitions in atoms, ions, or molecules (Raga et al. 1990). HH 47C traces the counterflow where it emerges from the visually opaque globule. HH 46/47 is associated with an ~0.3 pc-long molecular outflow with an H_2 mass $M_{out} \approx 0.8$–$3.2\ M_\odot$ confined to the boundaries of the cloud and to radial velocities less than ±40 km s^{-1} (van Kempen et al. 2009). The Atacama Large Millimeter Array (ALMA) shows that most of the high-velocity CO traces a swept-up shell along the walls of the red-shifted counterflow cavity (**Figure 1**; Arce et al. 2013). Shock-excited H_2 traces a prominent counterjet invisible at visual wavelengths as well as the wide-angle outflow cavity coincident with CO emission (Noriega-Crespo et al. 2004, Velusamy et al. 2007). Several CO knots along the counterjet toward the southwest may indicate quasi-periodic mass ejections from the source.

Herschel observations of mid-IR CO lines indicate emission from rotational levels up to $J_u = 30$, which is >2,500 K above the ground state. The CO spectral energy distribution can be subdivided into a cool ~100-K component originating in the cloud and protostellar envelope with emission peaking at $J_u \sim 3$ and extending to $J_u \sim 10$, an ~300-K UV-heated component formed in the outflow cavity walls in the range of $4 < J_u < 20$, and an ~700-K component heated by shocks that dominates $J_u \geq 20$. *Herschel* also detected OH, [OI], and [CII] (van Kempen et al. 2010, Nisini et al. 2015).

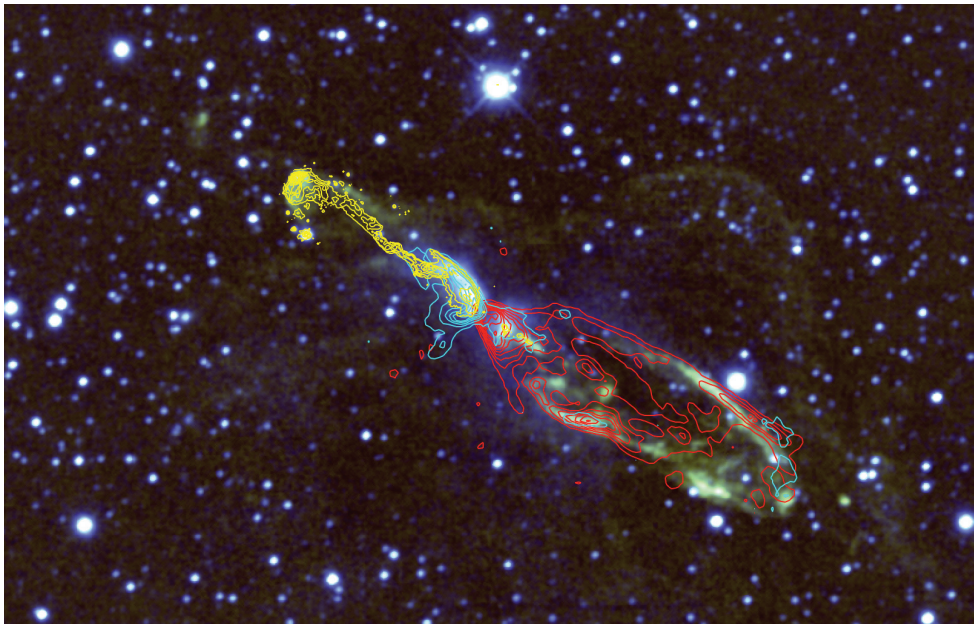

Figure 1

The inner part of the HH 46/47 system contains a small molecular outflow confined to the boundaries of the ESO 216-6A globule. The background image shows 2.12-μm H_2 emission (*light green*) observed with a 1%-bandwidth filter. Yellow contours show the location of the [SII] jet. The molecular outflow imaged with ALMA in the $J = 1$–0 CO line is shown in cyan and red contours. Blue-shifted emission from $V_{LSR} = -6.8$ to -1.3 km s^{-1} is shown in cyan, and emission from $V_{LSR} = +1.3$ to $+6.7$ km s^{-1} is shown in red. A small, blue-shifted secondary outflow extends from the source region toward the southeast. A visual wavelength image of this flow in [OII], Hα, and [SII] is shown in Reipurth & Bally (2001; see also **Figure 2**). The CO data was adapted from Arce et al. (2013) with permission of the author; it was combined with a near-IR image obtained by the author. The near-IR image was obtained with the National Optical Astronomy Observatory's (NOAO's) Extremely Wide-Field Infrared Imager (NEWFIRM) on the Blanco 4-m telescope by the author.

Garcia Lopez et al. (2010) used near-IR spectroscopy of [FeII] and H_2 to measure physical properties, finding radial velocities ranging from -230 to $+100$ km s^{-1} in the ionized component of the inner jet, electron densities $n_e \approx 4{,}000$ to 6,000 cm^{-3}, and mass-loss rates $\dot{M} \approx 0.5$ to 2×10^{-7} $M_\odot$ year^{-1} in the high-velocity component within a few thousand astronomical units of the source. The H_2 emission shows only one velocity component close to the source, but reaches velocities up to 95 km s^{-1} downstream. Analysis of the near-IR H_2 lines indicates that this emission originates from gas with $T_{gas} = 2{,}000$–$2{,}800$ K. These parameters are similar to other low-mass Class I outflows.

The outflow has broken out of its natal cloud to power a pair of large bow shocks, HH 47NE and HH 47SW, separated by over 2.6 pc and located more than 1.3 pc from the source (**Figure 2**). Thus, this outflow joins the growing list of parsec-scale HH flows (Stanke et al. 1999, Reipurth & Bally 2001).

2.2. Morphologies

Protostellar outflow morphologies range from jets to less-collimated bipolar lobes to quasi-spherical winds (Reipurth & Bally 2001; Arce et al. 2011, 2013; Nakamura et al. 2012). The

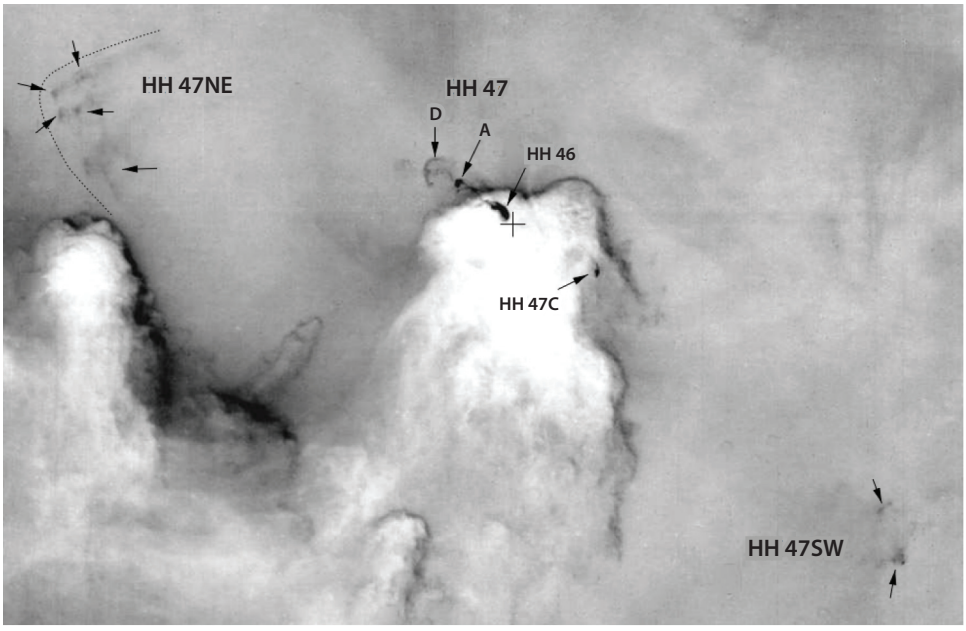

Figure 2

A continuum-subtracted, narrow-band Hα image showing the parsec-scale HH 46/47 outflow. The + symbol marks the location of the driving source. Reprinted from Stanke et al. (1999) with permission.

primary winds and jets emerge from YSOs with velocities ranging from a few km s^{-1} to over 10^3 km s^{-1}. The lowest velocities are observed in subparsec outflows from young brown dwarf stars such as the 0.046-$L_\odot$ GM Tau (Phan-Bao et al. 2014a,b) and molecular jets from first hydrostatic cores (FHSCs) such as Barnard 1b in Perseus (Gerin et al. 2015), whose compositions are mostly molecular with a low ionization fraction. Dunham et al. (2011) found a 0.06-pc-long, bipolar outflow with a maximum velocity of only ~2.9 km s^{-1} from a very low luminosity object, the $L \sim 0.01$-$L_\odot$ Per-Bolo 58 thought to be an FHSC with a mass of only 0.11 ± 0.04 $M_\odot$. Other FHSC candidates have small outflows (Price et al. 2012, Takahashi et al. 2013, Tsitali et al. 2013, Gerin et al. 2015).

Brown dwarf stars: stars in the range of $\sim 0.01 < M < 0.08$ $M_\odot$

First hydrostatic core (FHSC): a condensed object forming in a prestellar core

Standard high-velocity (SHV) component: component in the millimeter line profiles of outflows; $V \leq 50$ km s^{-1} with respect to the velocity of the cloud; sometimes subdivided into low-velocity and high-velocity around $V \approx 10$ km s^{-1}

Outflows from embedded Class 0 YSOs also tend to be much less than 1 pc in length and predominantly molecular. Class 0 YSOs often drive powerful molecular outflows with mass-loss rates up to $\dot{M} \sim 10^{-5}$-$M_\odot$ year^{-1} bright in CO, H_2O, OH, and sometimes SiO. Their primary jet or wind velocities range from 50 to 150 km s^{-1}. Shocks are most visible in the transitions of H_2 as MHOs. HH objects, if present, are dim and obscured. The HH 211 outflow, which originates from a 0.06-$M_\odot$ YSO near IC 348 in Perseus, is a good example (Lee et al. 2000, 2009, 2014; Tappe et al. 2012). The jet is bright in CO, SiO, and H_2 and is surrounded by a shell of swept-up molecular gas that constitutes the standard high-velocity (SHV) line wings at low radial velocities ($\Delta V_{\rm radial} \sim 2$–$10$ km s^{-1}) with decreasing amounts at $\Delta V_{\rm radial} \sim 10$–$50$ km s^{-1}. It contains dim HH objects confined to the end of the jet where it impacts the cloud. HH 212 in Orion is a slightly more evolved flow from a 0.3-$M_\odot$ Class 0 source (Zinnecker et al. 1998; Lee et al. 2006, 2007, 2008; Codella et al. 2007). Podio et al. (2015) obtained ALMA observations of SO and SO_2, and Codella et al. (2014) measured the outflow properties in CO $J = 3$–2. Outflowing molecular gas is only found at the base of the outflow with no molecules associated with the MHOs and dim HH objects found at the ends of the H_2 flow. Recent wide-field surveys of H_2 emission have led

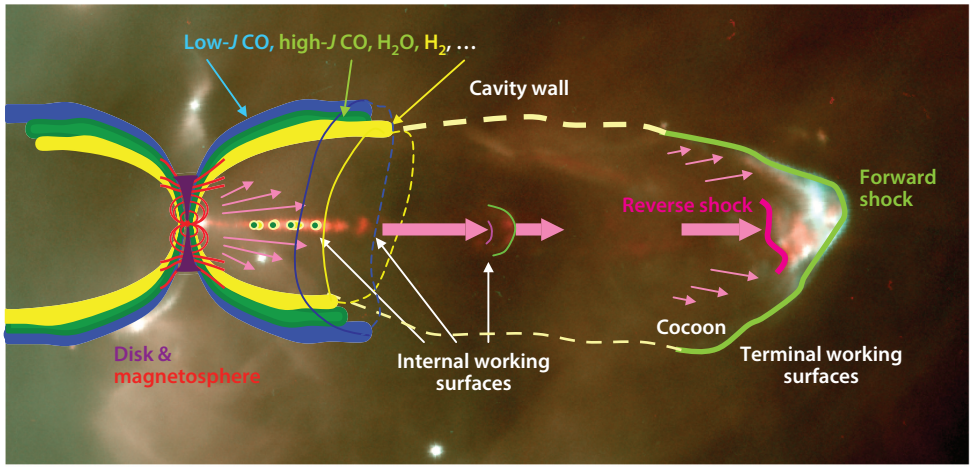

Figure 3

A cartoon showing the main components of a protostellar outflow lobe. The sizes of the disk (*purple*), the poloidal component of the disk and stellar magnetic fields (*red*), and the biconical molecular outflow are greatly exaggerated. The youngest outflows are compact, consisting of swept-up molecular shells powered by jets containing molecules. As they break out from their parent cores and grow to parsec scales, outflows become predominantly atomic or ionized and traced by Herbig-Haro (HH) objects. Molecules are usually confined to the outflow cavity walls near the source young stellar object but can also trace jets in the youngest flows. Thick, colored bands mark cavity shocks and UV-heated gas along the cavity walls, and spot-shocks mark supersonic velocity variations in the jet. Forward shocks are in bright green, and reverse shocks in magenta in both the terminal and internal working surfaces. Low-*J* CO is shown in blue, high-*J* CO in green, and shock-heated H_2 in yellow. The dashed, yellow line shows the predominantly atomic or ionized cavity wall. The underlying image shows a close-up of HH 34 and its driving jet in Hα (*cyan*) and [SII] (*red*).

to the discovery of hundreds of MHOs (Ioannidis & Froebrich 2012a,b; Lee et al. 2012, 2013; Froebrich et al. 2015).

More evolved Class 0 and Class I YSOs exhibit extremely high-velocity (EHV) component jets and bullets in the inner part of the outflow along with slower, wider-angle SHV molecular outflow lobes whose extents are confined to the parent cloud. Chains of HH objects often extend parsecs from their sources. Examples include the cluster of outflows emerging from the dark cloud Lynds 1448 located at the western end of the Perseus molecular cloud. The sources, L1448-mm, L1448 IRS2, and L1448 IRS3, each power molecular EHV jets surrounded by SHV lobes on subparsec scales. Deep visual wavelength images trace these outflows to chains of HH objects located parsecs away (Bally et al. 1997, Eislöffel 2000, Wolf-Chase et al. 2000).

Figure 3 shows a cartoon illustrating a typical outflow. Outflow shells, where most molecules are seen, surround low-density cavities (or cocoons) filled by wide-angle winds and shocked jet material. In the absence of winds, cavities can be formed by the sideways splash of shocked jet fluid produced by ejection-velocity variations. Shocks excite atoms, and molecules if present, and ionize some species. In the absence of external radiation, emission by the shocked medium renders jets visible. The supersonic expansion of the swept-up shell into the medium can produce additional low-velocity cavity-shocks that evaporate H_2O from grains and excite transitions of H_2, CO, and other molecules. UV from the YSO can dissociate H_2O to produce OH and excite high-*J* CO. Shear flows along the cavity wall can produce a complex of vortices and localized spot-shocks (Mottram et al. 2014).

Extremely high-velocity (EHV) component: component with $V > 50$ km s^{-1}

The leading edge of an outflow forms a terminal working surface (**Figure 3**) where the ambient material is swept up into a shock-compressed layer in a process called prompt entrainment. Flow velocity variability is responsible for chains of complex internal shock structures in which shock speeds are generally much lower than the bulk motion of the flow. Shear between the jet and cocoon, and along the cavity walls, can lead to Kelvin-Helmholtz instabilities and a turbulent interface, transferring momentum from the outflow to the surrounding medium in a process called steady entrainment.

Some outflows and jets are rendered visible by ionizing radiation from nearby massive stars (Cernicharo et al. 1998, Bally & Reipurth 2001a, Bally et al. 2006a). Their properties can be determined using photoionization models developed for the analysis of ionized nebulae. Visual wavelength emission lines such as Hα are sensitive to small emission measures, enabling the detection of faint jets with mass-loss rates less than 10^{-9} $M_\odot$ year^{-1} (Reipurth et al. 2010). Faint externally irradiated Hα jets originating from stars located parsecs from the closest molecular cloud indicate that weak outflow phenomena can last for millions of years. The 3- to 4-Myr-old σ Orionis cluster contains at least five externally irradiated jets powered by low-mass stars in the cluster (Reipurth et al. 1998a, Andrews et al. 2004, Riaz et al. 2015).

Many YSOs exhibit radio continuum emission (Tobin et al. 2015). Centimeter, millimeter, and submillimeter interferometry with Jansky Very Large Array (JVLA), Submillimeter Array (SMA), Combined Array for Research in Millimeter-wave Astronomy (CARMA), Northern Extended Millimeter Array (NOEMA), and ALMA provide arcsecond and subarcsecond continuum images and data cubes of the line emission, matching or bettering the resolution of HST and ground-based adaptive optics. A few outflows have been detected in the 21-cm line of HI such as NGC 2071 (Bally & Stark 1983), the SVS13 outflow in NGC 1333 (Rodriguéz et al. 1990), and DR21 (Russell et al. 1992). However, background emission from the Galaxy is too widespread to make this line a generally usable tracer of outflows. UV lines such as Lyman-α have only been observed from a few outflows (Devine et al. 2000, Grady et al. 2000) because they can only be observed from space and in low-extinction environments.

2.3. Evolutionary Trends

Mass loss traced by molecular jets increases with accretion rate (**Figure 4**). But, as sources evolve from Class 0 to I, outflow power declines and the primary winds tend to become faster as well as increasingly atomic and less molecular (**Figure 5**). The momentum injection rate increases with the source luminosity, envelope mass, and total outflow mass (**Figure 6**), but declines as sources transition from Class 0 to I. As flows grow larger than the size of their parent core, clump, or cloud, they blow out and dump momentum into the surrounding ISM. As YSOs evolve, the velocity of their primary winds or jets tends to increase, transitioning from predominantly molecular to mostly atomic and partially ionized plasma. The jets, the splash of material expanding orthogonal to the flow from internal shocks, and slower, wider-angle winds inflate an ever-widening cavity in the cloud, sweeping up, shocking, and accelerating shells of molecules that exhibit a wide range of temperatures from tens to thousands of Kelvin. Swept-up shells traced by CO become less prominent as they widen, sweep up more mass, and decelerate. As outflows break out of their parent cloud cores, their internal shocks are best traced by chains of HH objects.

Outflow cavities also tend to become wider as flows age (Offner et al. 2011). The base of the HH 366 flow from Barnard 5 is a good example (Yu et al. 1999, Zapata et al. 2014). The brightest emission from material in the cavity is often confined to narrow jets or HH objects along the cavity axis. The swept-back wings of high-excitation bow shocks extending orthogonal to the low-excitation jet in systems such as HH 46/47 indicate the presence of a lower-density, slower-moving fluid in the outflow cavity interior. The cavity interiors are filled with either lower-density,

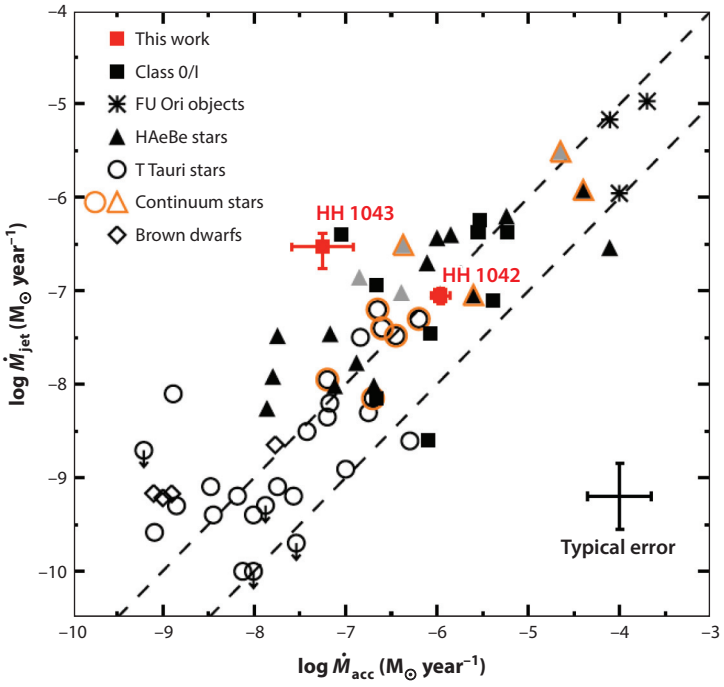

Figure 4

The relation between mass-loss rate in stellar jets, $\dot{M}_{jet}$, versus accretion rate onto the young stellar objects, $\dot{M}_{acc}$. The dashed lines indicate ratios of $\dot{M}_{jet}/\dot{M}_{acc} = 0.1$ and 0.01. The mass-loss rates may be lower bounds as discussed in the text. The data in this plot were taken from Ellerbroek et al. (2013).

less-collimated winds originating at larger disk radii than the highly collimated jets or gas that has expanded orthogonal to the jet axis in side-splashing bow shocks formed where faster ejecta catches up to older, but slower, matter in the jet.

By the early 2000s, over 1,000 HH objects were known (refer to **http://vizier.u-strasbg.fr/viz-bin/VizieR?-source=HH**) (Reipurth & Bally 2001). Molecules in outflows from Class I YSOs are generally only observed close to the source, whereas wide-field images show that HH objects can often be found at distances of many parsecs (Ogura 1991, Bally & Devine 1994, Devine et al. 1997, Eislöffel & Mundt 1997, Reipurth et al. 1997a). Near their sources, the radial velocities and proper motions of HH objects are often an order of magnitude greater than the velocities of the SHV molecular emission, suggesting that HH objects trace shocks in the primary wind or jet, whereas molecules mostly trace swept-up gas. HH object radial velocities and proper motions tend to decrease with distance from the source (Devine et al. 1997). The determination of outflow parameters from shock radiation is limited to gas that just passed through a shock within a cooling time and is complicated by the nonlinear physics.

The morphology of HH objects and MHOs indicates that outflows have large-amplitude variability in mass-loss rate and ejection velocity, and some show evidence for changes in the ejection direction and degree of collimation (Reipurth & Bally 2001). Most flows contain multiple shocks along their axes with gaps whose lengths increase with increasing distance from the source YSO. Within about 0.1 pc of their sources, a few percent of outflows exhibit highly collimated jets in the radio continuum, as HH objects, or MHOs with chains of closely separated low-excitation knots indicating shock velocities of a few tens of km s^{-1} in a medium moving with

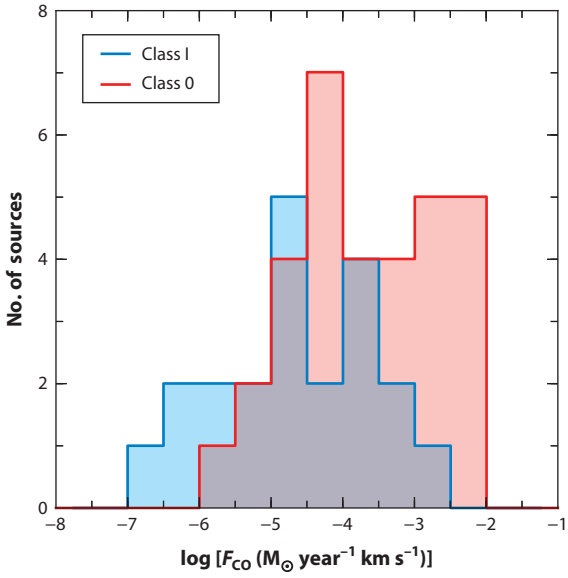

Figure 5

A histogram of momentum injection rates for Class 0 and 1 low-mass young stellar objects. Adapted from Mottram et al. (2016) with permission.

speeds of 100 to over 400 km s^{-1}. In contrast to the low-excitation shocks close to the outflow source, distant shocks tend to have higher excitation, indicating increasingly large differences in the speeds of the colliding fluids. These features are best explained as variability in the mass-ejection velocity (Reipurth et al. 2002a; Raga et al. 2002, 2011a). The distribution of shocks in most flows indicates that low-amplitude velocity variations occur on short timescales, whereas large-amplitude changes occur on long timescales. The modulation spectrum of the ejection velocity may resemble $1/f$ frequency-flicker noise processes. These fluctuations may indicate episodic accretion accompanied by variations in mass-loss rate and primary-wind ejection velocity.

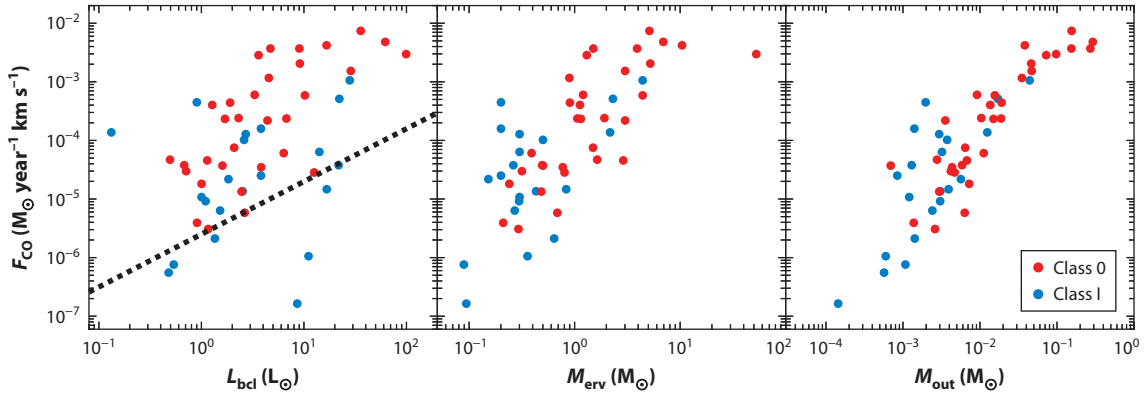

Figure 6

The momentum injection rates as functions of source bolometric luminosity, envelope mass, and outflow mass determined from CO $J = 3$–2 for Class 0 and 1 low-mass young stellar objects. Adapted from Mottram et al. (2016) with permission.

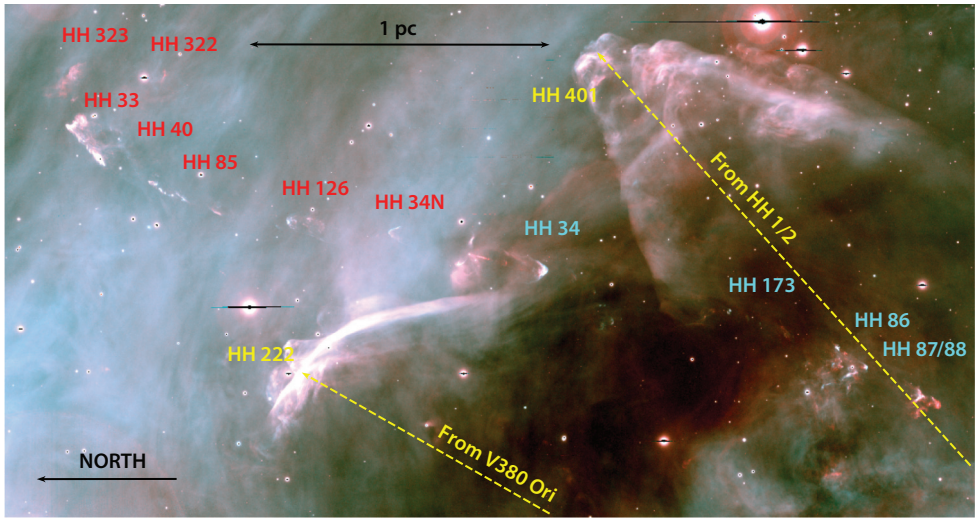

Figure 7

A narrow-band Hα (*cyan*) and SII (*red*) image showing the 2.7-pc-long HH 34 outflow complex in Orion A stretching from upper left to lower right. Red and blue labels indicate red-shifted and blue-shifted components, respectively. The giant HH 401 (*top right*) and HH 222 (*bottom middle*) bow shocks originate from sources located toward the southeast (*lower right*). North is toward the left, east is toward the bottom. Based on data from Reipurth et al. (2013).

Some outflows exhibit changes in the ejection direction and degree of collimation. Flow orientation variability produces curved chains of shocks between the terminal working surface and the source. When both sides of the flow are seen, slow orientation changes result in S-shaped point symmetry (Masciadri et al. 2002). A subset of HH outflows and jets exhibit C-symmetric bends, indicating that the source is moving through a medium (Bally & Reipurth 2001) or that the medium is flowing past the source (e.g., HH 1045 in NGC 1977; Bally et al. 2012b). The so-called LL Orionis objects in the Orion and Carina nebulae appear to be extreme examples of jet deflection by side winds (Bally et al. 2006a, Smith et al. 2010).

The S-symmetric HH 34 system illustrates many general properties of outflows from low-mass Class I YSOs. **Figure 7** shows the 2.7-pc-long chain of HH objects associated with HH 34 in the Orion A cloud (Bally & Devine 1994, Devine et al. 1997). As is the case with HH 46/47, the source of HH 34, a Class I protostar, powers a 2 arcmin (0.3-parsec) molecular outflow (Chernin & Masson 1995). A highly collimated, low-excitation, knotty jet with a mean radial velocity of approximately -100 km s^{-1} and proper motions of $\sim$200 km s^{-1} emerges from the source. Jet proper motions decline to $\sim$160 km s^{-1} about 30 arcsec away, where the jet fades (Raga et al. 2012a). A pair of higher-excitation bow shocks, HH 34 and HH 34N (**Figure 7**), are symmetrically located $\sim$90 arcsec from the source on both sides. A chain of more widely spaced shocks with decreasing velocities terminates in HH 33/40 to the north and HH 87/88 to the south, marking the ends of a 2.7-pc-long flow. Deceleration of fragmented ejecta by the surrounding medium may be responsible for the declining velocity with increasing distance from the source (Cabrit & Raga 2000). Multimode variations in the ejection velocity of the jet can explain the observed morphology and proper motions (Raga & Noriega-Crespo 1998; Raga et al. 2002, 2012b). Point-symmetric orientation changes are most likely an indication of forced precession of the stellar and/or disk rotation axes. Possible causes of forced precession include accretion flows that change direction

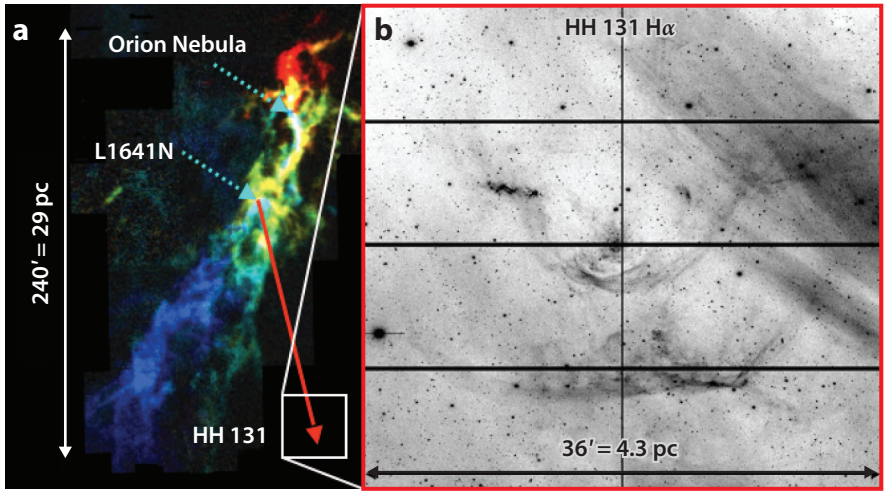

Figure 8

(*a*) A ^{13}CO image of the Orion A giant molecular cloud showing the locations of the L1641N cluster suspected to be the source of HH 131. Colors indicate radial velocities from $V_{LSR} = 2$ to 14 km s^{-1} (*blue* to *red*). (*b*) A narrow-band Hα image of HH 131 obtained with the Mosaic CCD on the Mayall 4-m telescope on Kitt Peak. The black grid indicates gaps in the CCD. The CO data is from Bally et al. (1987); the unpublished Hα image was taken by the author in 2001 with the Blanco 4-m telescope at the Cerro Tololo Inter-American Observatory.

with time or the torques generated by a binary companion whose orbital plane is tilted with respect to the disk associated with the outflow source (Bally & Reipurth 2001).

Figure 7 also shows the giant HH 401 bow shock, which together with HH 402 forms the ∼5-pc-long flow powered by HH 1 and 2 (Ogura 1995). HH 1/2 is also only associated with a 0.3-pc molecular flow (Chernin & Masson 1995). HH 222 is powered by the quadruple Herbig Be star V380 Ori ∼3 pc to the southeast (Reipurth et al. 2013). Another example of a giant HH outflow from a YSO with subparsec molecular lobes includes HH 111 in the Orion B cloud, which powers HH 113 and 311, which are separated by 7 pc (Reipurth et al. 1997a).

The largest outflows have lengths of tens of parsecs, comparable with the dimensions of giant molecular clouds (GMCs). The giant HH 131 bow shock (**Figure 8**), located more than a degree west and two degrees south of the L1641N cluster in the Orion A cloud, has a diameter of about 30 arcmin or about 4 pc at the assumed distance of ∼400 pc to Orion (Ogura 1991). Deep Hα and [SII] images have identified a chain of HH objects, HH 61/62, HH 127, HH 479, and HH 480, between the L1641N cluster and HH 131, indicating a giant outflow with a blue-shifted outflow lobe having a projected length of over 17 pc and extending south-southwest from the cluster. North-facing bow shocks HH 403 to HH 406 located north-northeast of L1641N may trace a counterflow, implying an overall outflow projected length greater than 20 pc (Reipurth et al. 1998b). **Figure 9** shows a comparison of outflow lengths in different tracers.

2.4. Shock Structure

Collimated flows tend to form bow shocks in places where they ram slower or stationary media. As winds or jets slam into their surroundings, a forward shock accelerates, heats, and compresses the medium. Between this forward shock and the source, a reverse shock decelerates, heats, and

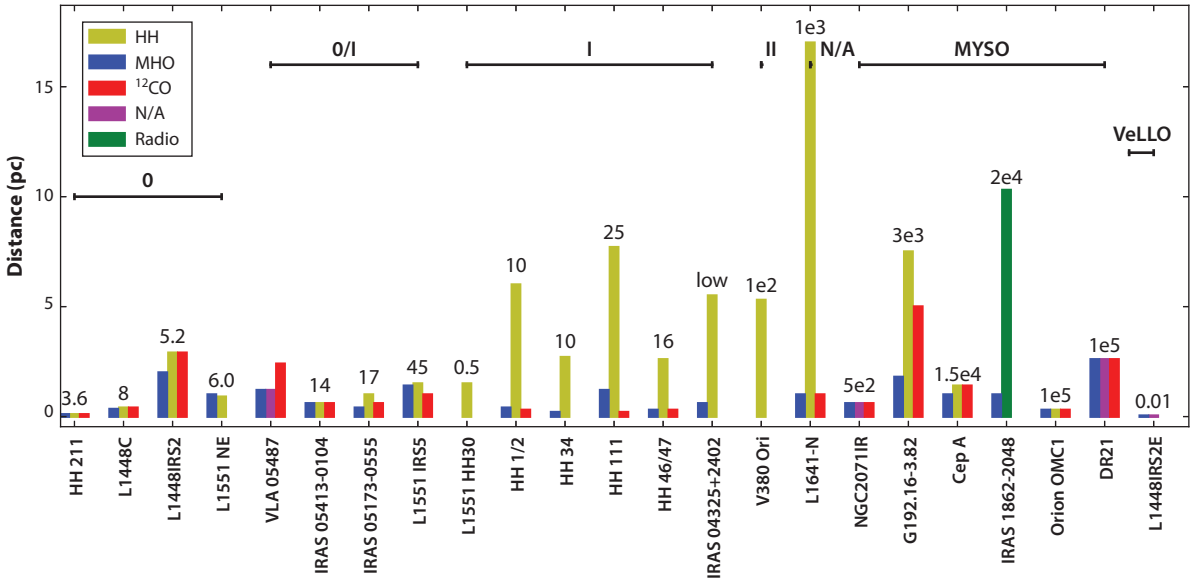

Figure 9

A comparison of the lengths of outflows traced by molecules such as CO, molecular hydrogen objects (MHOs), and Herbig-Haro (HH) objects for a subset where all three tracers have been observed. Numbers above each colored bar indicate the luminosity in $L_\odot$. The luminosity class is indicated above the horizontal bars. N/A indicates "not available." The driving source of the giant outflow in the L1641N cluster has not been directly identified, nor have any HH objects been found in DR21 owing to extinction. Abbreviations: MYSO, massive young stellar object; VeLLO, very low luminosity object.

compresses the outflow. In the center-of-mass frame of this shock-sandwich, the ram pressure of the colliding fluids is given by $P_{\rm ps} \approx \rho_i V_i^2 + B_i^2/8\pi$, where the subscripts refer to each preshock fluid that enters the shock with velocity V_i and matter density $\rho_i = \mu_i m_H n_i(H)$. For reviews of shocks, see McKee & Hollenbach (1980), Hollenbach & McKee (1989), McKee & Draine (1991), and Draine & McKee (1993). The temperature immediately behind a shock is given by $T_{\rm ps} \sim 3\mu m_{\rm H} V_s^2/16k$, where μ is the mean molecular weight ($\approx$2.8 per H_2, $\approx$1.4 per atomic hydrogen, or $\approx$0.7, where H is ionized), $m_{\rm H}$ is the mass of hydrogen, and V_s is the shock speed. For $20\,{\rm km\,s^{-1}} < V_s < 10^3\,{\rm km\,s^{-1}}$, the immediate postshock temperatures are $10^4 < T_{\rm ps} < 10^7$ K, and H will be ionized by collisions. In this temperature range, the cooling curve for Solar metallicity is $\Lambda \sim 0.3-4\times10^{-22}\,{\rm erg\,sec^{-1}\,cm^3}$. Given the interstellar cooling curve Λ, a postshock hydrogen number density $n_{\rm H}$, and a temperature $T_{\rm ps}$, the cooling time is approximately $t_{\rm cool} \sim 1.5 n_{\rm H} k T_{\rm ps}/\Lambda n_{\rm H}^2 = 9\mu m_{\rm H} V_{\rm H}^2/32\Lambda n_{\rm H}$. Interpolation of the cooling curves for Solar metallicity (Draine 2011) gives $t_{\rm cool} \approx 8 V_{30}/n_{100}$ years for $30 < V_s < 100$ km s^{-1} and $t_{\rm cool} \approx 1.1 \times 10^3 V_{300}^{3.4}/n_{100}$ years for $10^2 < V_s < 10^3$ km s^{-1}. Here V_{30} and V_{300} are the shock speeds in units of 30 and 300 km s^{-1}, respectively, and n_{100} is a typical postshock proton density in units of 100 cm^{-3}. The cooling length, which is a measure of the separation of the shock and the radiating region, is given by $L_{\rm cool} \sim V_s t_{\rm cool} = 9\mu m_{\rm H} V_s^3/32\Lambda n_{\rm H}$. Thus, $L_{\rm cool} \sim 50 V_{30}^2 n_{100}^{-1}$ AU for $30 < V_s < 100$ km s^{-1} and $L_{\rm cool} \sim 0.34 V_{300}^{4.4} n_{100}^{-1}$ pc for $10^2 < V_s < 10^3$ km s^{-1}. Objects such as HH 46/47 have $n_H \sim 10^3$ cm^{-3}. In dense gas, $t_{\rm cool}$ is short and postshock gas tends to be far from local thermodynamic or ionization equilibrium. However, in the low-density regions with $n < 10$ cm^{-3}, where HH objects are often found, fast shocks can lead to long postshock cooling times and parsec-scale cooling lengths.

The cooling function depends nonlinearly and strongly on the fractional ionization, temperature, and density. At temperatures below 10^4 K, cooling decreases by 2 to 4 orders of magnitude. Recombining hydrogen can only emit ~14-eV photons once because at temperatures below 10^4 K, collisions cannot reionize or excite the $n = 2$ or higher energy levels of H. Thus, emission from most HH objects and HII regions is dominated by ~2–3-eV ground-state transitions of species with relatively low abundances compared to H such as [SII], [OI], [OII], [OIII], and [NII], which originate in the partially ionized recombination zone and cooling layer behind shocks. For each recombining H-atom, the upper states of these ions can be excited thousands of times by collisions before recombining to their neutral states. As the gas recombines and cools, and the ionization fraction drops to below a few percent, cooling becomes dominated by the mid-IR fine-structure lines of the most abundant species such as 63-μm [OI] and 157-μm [CII].

If molecules survive the shock or are entrained or formed by chemical processes, they will dominate cooling (Herczeg et al. 2012, Karska et al. 2013, Flower & Pineau des Forêts 2015). Important molecular coolants include CO and H_2O, which is liberated from ice mantles on grains in moderate velocity shocks; OH, which is produced by photodissociation of H_2O; and H_2. At $T < 100$ K, H_2O freezes onto grains. In cold clouds below $T < 10$ K, CO, CO_2, and NH_3 also freeze. UV radiation can activate solid-phase chemical reactions in these ice mixtures and produce complex organics such as CH_3OH (van Dishoeck et al. 2013). The CO, CO_2, and NH_3 can re-enter the gas phase when grains pass through shocks with V_s greater than a few km s^{-1}. Observations show that shock speeds of tens of km s^{-1} are needed to desorb H_2O ice, methanol, and other complex organics (Bjerkeli et al. 2012, Busquet et al. 2014). Shocks with speeds of many tens of km s^{-1} can sputter refractory grains, increasing the gas-phase abundance of SiO by orders of magnitude compared to quiescent clouds (Anderl et al. 2013).

The near-IR rovibrational transitions of H_2 and CO radiate at a characteristic temperature of a few thousand Kelvin and trace shocks where primary winds transfer momentum to the swept-up molecular gas. As temperatures drop, [OI] and the rotational states of H_2O, CO, and OH dominate cooling; below 100 K, CO dominates. *Herschel* detected high-J transitions of these species in outflow gas with temperatures of a few hundred to a few thousand Kelvins (Goicoechea et al. 2012; Karska et al. 2014a,b). These studies show that across the full range of outflows from low- to high-mass YSOs, the CO rotational diagrams have remarkably similar temperature components. CO rotational line intensities can be almost universally fit with three power-law fits giving $T_{ex} \sim 100$ K for $J_u = 1$–12, ~300 K for $J_u = 13$–25, and ~700 K for $J_u > 25$ (Goicoechea et al. 2012). The rotational diagrams are similar for low-mass Class 0 and I sources.

Cooling rates increase with density. Thus, density fluctuations in postshock gas tend to grow, resulting in fragmentation into dense clumps. Such cooling instabilities may explain the complex structure of objects such as HH 2 in which dense, fast-moving clumps run into a slower, tenuous medium form forward-facing bows, and slower-moving clumps overtaken by a faster, lower-density medium form backward-facing bows (Raga et al. 2011b, 2015; Hartigan et al. 2011). These clumps may have formed a long time ago as the gas passed through shocks closer to the source.

Shocks with $V_{shock} \geq 60$ km s^{-1} propagating into mostly neutral gas produce a thin zone radiating only in the H-recombination lines. A narrow, rest-velocity component forms where hydrogen in the stationary medium is collisionally excited by the onrush of fast postshock protons. A high-velocity tail of emission extending up to the shock speed is formed by these fast protons exchanging electrons with the neutrals. Charge exchange tends to leave the resulting moving atoms in excited states that radiate H-recombination lines. These Balmer filaments lack emission by forbidden transitions and have dimensions of order $1/n\sigma \sim 0.1\sigma_{-15}^{-1} n_3^{-1}$ AU, where σ_{-15} is a typical cross section for ion-neutral collisions in units of 10^{-15} cm^{-2} and n_3 is the ambient medium

density in units of 10^3 cm^{-3}. Although Balmer filaments mark the location of the shock front, most of the H-recombination line flux originates in the recombination zone behind the Balmer filament where the forbidden line emission also originates. The separation between these zones can be used to measure the cooling length and, with the aid of velocities, the cooling time.

Shocks with $V_s \geq 100$ km s^{-1} emit UV radiation that propagates both up- and downstream, ionizes low-excitation species, and maintains elevated temperatures in the pre- and postshock zones. Shocks with $V_s > 400$ km s^{-1} produce X-rays (Pravdo & Tsuboi 2005, Grosso et al. 2006, Pravdo et al. 2009, Schneider et al. 2009).

In the presence of strong magnetic fields, Alfvén waves can preaccelerate the charged component, allowing ion-neutral drag to produce enough heat to erase the discontinuities in density, temperature, and pressure that characterize HD shocks. When discontinuities exist in the fluid, the shock is referred to as a jump or J-shock; when magnetic fields smooth out the discontinuities and the fluid variables change slowly, the supersonic disturbance is referred to as a continuous or C-shock. Although there are no direct B-field measurements in protostellar outflows, equipartition suggests that field strengths in the postshock plasma could be as large as $B \sim (8\pi\rho)^{0.5} V_s \sim 2 n_3^{0.5} V_{100}$ mG, where n_3 is the hydrogen density in units of 10^3 cm^{-3} and V_{100} is the shock speed in units of 100 km s^{-1}. Magnetic fields decrease the postshock temperature dramatically as the field is compressed. Observations show that in most outflows, molecules such as H_2 and CO can survive shocks up to speeds of 20 to over 80 km s^{-1}.

P Cygni line profiles: the mass-losing supergiant P Cygni exhibits blue-shifted self-absorption in its emission lines, indicating the presence of an outflowing wind

Extended green object (EGO): indicates shocks, probably radiating in the v = 0–0 rotational states of H_2 with possible contributions from the 4.6-μm CO fundamental vibrational bands

2.5. Mid-IR to Submillimeter Diagnostics

Most of the luminosity of Class 0 and I YSOs and molecular outflows emerges in the mid-IR to submillimeter wavelength range. ISO spectra measured the fluxes of pure rotational states of H_2; a variety of fine-structure cooling lines; high-lying transitions of common molecules, such as CO and OH, and species unobservable from the ground, such as H_2O, 63-μm [OI], and 157-μm [CII]; and the mid-IR continuum emission where most of the luminosity from outflows peaks (Smith et al. 1998, van den Ancker et al. 1999, Rosenthal et al. 2000, Gålfalk et al. 2004). These observations led to more complete analyses of the large number of observable lines from shocks. The penetrating power of the mid-IR enables the identification of flow components hidden at shorter wavelengths (Henning et al. 2000, Molinari et al. 2000, Bourke 2001, Froebrich et al. 2002, Molinari & Noriega-Crespo 2002). ISO spectra of the OMC1 BN/KL region in the 44- to 188-μm wavelength range detected over 150 lines (Lerate et al. 2006, 2008). Mid-IR pure rotational CO lines originate from states up to $J_u = 39$, indicating that this emission traces hot, $T > 3{,}000$ K, dense gas with $n(H_2) \approx 3 \times 10^4$ to 10^6 cm^{-3}. The P Cygni line profiles confirmed that most of this emission arose from high-velocity outflow. States with $18 < J_u < 25$ trace warm, $T \sim 200$ K, gas from $n(H_2) \sim 10^7$ cm^{-3} hot cores.

Spitzer imaging from 3.6 to 24 μm of dozens of star-forming complexes detected tens of thousands of YSOs by means of their IR-excess emission. Outflows with strong 2.2-μm near-IR H_2 lines (MHOs) were found to be also bright at 4.5 μm. These images are frequently displayed with the 3.6-μm band in blue, the 4.5-μm band in green, and the 8.0-μm band in red. Consequently, shocks detected at the 4.5-μm band are rendered green, and the term extended green object (EGO) came into common use in describing *Spitzer*/IRAC-detected outflow candidates (Cyganowski et al. 2008). *Spitzer*'s InfraRed Spectrometer (IRS) observed the mid-IR v = 0–0 H_2 lines from many outflows. Tappe et al. (2012) showed that the 4.5-μm excess in EGOs may trace either high-J pure-rotational transitions of H_2 or the 4.6-μm v = 1–0 fundamental vibrational band of CO.

The 63-μm line of [OI] is one of the most important coolants of atomic gas. *Herschel* imaged [OI] from the jets in L1448, NGC 1333-IRAS 4, HH 46, BHR 71, and VLA 1623, finding velocities

as high as 200 km s^{-1} and [OI]-derived $\dot{M}_{jet}(OI)/\dot{M}_{acc} \sim 0.05$–0.5 (Nisini et al. 2015). *Herschel* far-IR spectroscopy measured the cooling rate of postshock gas at wavelengths at which most of the energy injected by outflows emerges as radiation (Nisini et al. 2010a,b; Giannini et al. 2011). The far-IR and submillimeter spectra show that in addition to the low-*J* transitions of molecules such as CO, outflows contain warm and hot molecules with temperatures of several thousand Kelvins that radiate in high-*J* transitions. These far-IR measurements identified emission by important far-IR cooling lines, H_2O, OH, and metal-hydrides (see Gerin et al. 2016, in this volume). *Herschel* spectra show that hot CO and H_2O are major coolants of postshock molecular gas in the inner, molecular parts of outflows (Kristensen et al. 2010, 2011; Herczeg et al. 2012; Santangelo et al. 2013, 2014). The *Herschel* key program WISH (Water In Star-forming regions with Herschel; Tafalla et al. 2013) showed that H_2O emission has spatial structure and intensity distribution similar to H_2 and appears to be associated with $>10^2$-K gas in a high-pressure environment with a typical value of $P/k \sim 10^9$–10^{10} cm^{-3} K. However, the gas phase H_2O abundance with respect to H_2 is typically only about 3×10^{-7} (Karska et al. 2014b). The observed line profiles differ from model predictions for planar shocks (Flower & Pineau des Forêts 2010). San José-García et al. (2013, 2015) presented *Herschel*/HIFI observations of high-*J* CO and H_2O of 51 embedded YSOs drawn from the WISH program, including 26 low-mass, 6 intermediate-mass, and 19 high-mass objects. They find that the CO and H_2O line luminosities correlate with source luminosity over six orders of magnitude, and outflow properties increase smoothly over this entire range.

Goicoechea et al. (2015) presented *Herschel* spectra and maps of the BN/KL outflow and detected over 100 lines of water, OH, HCN, and CO. Transitions of CO up to $J_u = 48$ and excited water emission indicate molecular gas with $T_K \sim 2{,}500$ K and high H_2O abundances with $X(H_2O)/X(CO) > 1$ for shocks greater than ~25 km s^{-1}. The total luminosity in CO is 0.5% of the total far-IR luminosity, and most of the CO column density is in the warm component with $T_K \sim 200$ to 500 K. The water abundance in this component is low with $X(H_2O)/X(CO) < 0.01$. SOFIA continues to provide access to high-resolution spectroscopy in the mid- and far-IR and is starting to have a major impact (Eislöffel et al. 2012, Gómez-Ruiz et al. 2012, Gusdorf et al. 2015).

2.6. Determination of Physical Parameters

Measurements of masses, velocities, and momentum injection rates are fundamental for determining the roles of outflows in feedback, turbulence generation, and the disruption of the star-forming environment. However, each tracer only probes a limited range of properties and parameters. Although many observational techniques can be used to measure velocities, only a few allow reliable estimation of the density, column density, and mass of accelerated gas. Visual and near-IR emission lines trace the current locations of shocks. However, only the rate at which matter is actively processed through these shocks can be measured. External UV radiation can provide better constraints on masses because densities can be measured using the standard analysis applied to HII region plasmas. However, if the flow retains a neutral core, only lower bounds on mass can be derived.

The low-*J* millimeter and submillimeter transitions of common molecules provide relatively reliable estimates of column densities and masses in the cold component because these lines are easily excited at typical cloud temperatures. However, the determination of excitation temperatures, abundances, line opacities, and amounts of outflow gas hidden by the ambient cloud core because it has the same radial velocity comes with uncertainties of at least a factor of two each. Although high-velocity wings tend to be optically thin, at velocities within ~10 km s^{-1} of the line core, excitation temperatures and optical depths can be complex functions of location and

velocity. Most early studies adopted excitation temperatures around T_{ex} = 10–50 K. However, the intensities of high-*J* lines with *Herschel* (van Kempen et al. 2010; Yıldız et al. 2013, 2015) show that T_{ex} can be much greater and take on a range of values along each line of sight.

^{12}C/^{13}C ratio: this ratio is 89 in the Sun; in molecular clouds it varies from 89 to 40

Dunham et al. (2014) argue that previous studies of outflows underestimated optical depths and amounts of molecular mass and momentum in the low-radial-velocity parts of outflows hidden by the ambient cloud. Additionally, significant high-velocity emission can hide below the sensitivity limits of observations, and there are larger uncertainties in inclination angles. Dunham et al. (2014) suggest that masses and dynamical parameters must be revised upward by at least a factor of two for most sources, and possibly one to two orders of magnitude in a few cases. van der Marel et al. (2013) present a critical analysis of various mass and momentum injection rate analysis methods based on CO. They conclude that these parameters are uncertain by at least a factor of five.

Dunham et al. (2014) analyzed ^{12}CO and ^{13}CO transitions for both J = 2–1 and J = 3–2 emission of 17 outflows from low-mass YSOs and determined empirical fits to the ^{12}CO/^{13}CO ratio. In the J = 2–1 lines, the ratio of main-beam antenna temperatures varies as $T_{12}/T_{13} = (1.90 \pm 0.09)(V - V_{rest})^2 + 3.72 \pm 0.48$, and in the J = 3–2 lines the ratio varies as $T_{12}/T_{13} = (5.77 \pm 0.68)(V - V_{rest})^2 + 1.73 \pm 0.03$, where the velocities are in km s^{-1}. These ratios can be used to derive the opacity of the CO lines by assuming a ^{12}C/^{13}C ratio (Dunham et al. 2014, Maud et al. 2015b). The low-*J* ^{12}CO lines are opaque in the low-velocity components of the line wings, where most of the swept-up mass resides, but are optically thin in the high-velocity and EHV components. The high-*J* lines are often subthermally excited. For a descriptions of the methods used for the determination of column densities, outflow, masses, momentum injection rates, and mechanical luminosities, see Dunham et al. (2014), Yıldız et al. (2015), Maud et al. (2015b), and van der Marel et al. (2013).

Downes & Downes (2007) present numerical models of the jet-driven molecular outflow mass-velocity and intensity-velocity relations for low-*J* CO emission. The intensity-velocity relation can be fit with a power law with an index of approximately −1.5 at low velocities and from ∼4 to −6 at above 10 to 30 km s^{-1}. The rapid fall-off with velocity is observed and may indicate that molecules are subthermally excited or destroyed at high velocities. These effects can lead to underestimation of the ages and momentum injection rates.

Outflow mass and momentum injection rate estimates must also account for faster atomic and ionized components, especially in mature flows that have blown out of their parent clouds. Whereas in the youngest flows from Class 0 sources, atoms and ions likely constitute only a few percent of the mass, giant HH flows such as HH 34 (**Figure 7**), HH 46/47, or HH 111 tend to contain little molecular gas and only do so close to their sources. Most outflow mass and momentum is in atoms and ions. The ratio of the outflow mass-loss rate divided by the accretion rate, $f = \dot{M}_{out}/\dot{M}_{acc}$, which on the basis of low-*J* CO observations has often been taken to have a value of 0.01 to 0.3, may be larger with values over 1 in some cases (**Figure 4**). Thus, the momentum injection rates (**Figures 5** and **6**) may be lower bounds. A rough estimate of the mass in atoms and ions can be made by assuming that a low-density, interclump medium with a density n_{ICM} has been swept up by the observed shocks. The mass and momenta are then $M_{ICM} \sim \mu m_H n_{ICM} L D^2 \approx 0.03 n_1 L_{pc} D_{pc}^2$ ($M_\odot$) and $P \sim V_{out} M_{ICM} \approx 3 n_1 V_{100} L_{pc} D_{pc}^2$ ($M_\odot$ km s^{-1}), where n_1 is the ICM density in units of 1 cm^{-3}, L_{pc} is outflow length, and D_{pc} is its width (in parsecs), assuming the source is in the middle and the line-of-sight depth is the same as the projected width. The dynamic age is $\tau_{dyn} \sim L_{pc}/2V_{100} \approx$ 5,000 (years), where V_{100} is the mean ejecta velocity in units of 100 km s^{-1}. The mean momentum injection rate is given by $\dot{P} \sim P/\tau_{dyn} \approx 6 \times 10^{-4} n_1 D_{pc}^2 V_{100}^2$ ($M_\odot$ km s^{-1} year^{-1}). For flows such as HH 34, HH 46, and the giant flow from L1641N with D ∼0.2 to 2 pc, and $n_{ICM} \sim 1$ and 10 cm^{-3}, this estimate for $\dot{P}$ gives values from 2×10^{-5} to 2×10^{-2} $M_\odot$ km s^{-1} year^{-1}.

2.7. Launch and Collimation

X-winds: centrifugally launched MHD winds from open field lines of a stellar magnetosphere

Disk winds: centrifugally launched MHD winds from open field lines threading an accretion disk

The momentum injection rate of most outflows is orders of magnitude larger than the momentum in the source radiation fields. Thus, their launch is generally believed to involve magnetocentrifugal acceleration within a few astronomical units of a forming star by magnetic fields anchored in the dense inner parts of an accretion disk, from the interaction zone of the stellar magnetosphere with the disk gas and the disk field, or by open field lines in the stellar field. The small size of the launch and collimation region makes observations difficult (see Frank et al. 2014 for a recent review).

Accretion disks are supported by differential rotation close to the Kepler speed at each radius. Because YSOs accrete most of their mass from such disks and are convective, magnetic dynamos are expected to generate strong stellar fields whose pressure disrupts the inner disk. The Keplerian orbit period at the inner disk edge where the stellar magnetic field couples to the disk may regulate stellar spin (Königl 1991, Zweibel et al. 2006). Closed magnetic field lines guide matter from the inner edge of the disk to magnetic footprints on the stellar surface, usually at high latitudes. Accretion along such funnel flows spins up the star, which may increase the efficiency of the stellar dynamo, forcing the field to reach farther out into the disk. In X-wind models, matter picked up by open stellar field lines threading the inner edge of the accretion disk (~0.05 to 0.5 AU) is centrifugally accelerated as a wide-angle flow with speeds a few times the Kepler speed at the launch point. The magnetic torque resulting from the anchor point moving to larger disk radii and the torque of the X-wind tend to spin-down the star. For summaries of the theory of X-winds and disk winds see Shu et al. (2000), Shang et al. (2007), Pudritz et al. (2007), Mohanty & Shu (2008), Frank et al. (2014), and Li et al. (2014).

In disk wind models, open field lines inherited from the parent cloud are compressed by the gravitational collapse of the core and twisted by rotation (Königl et al. 2010, 2011). The disk field can be amplified by convection and shear in the disk, resulting in a twisted, pinched, helical hourglass configuration with open field lines tending to bend away from the direction to the YSO. Charged particles above or below the disk that end up on outward-bending field lines can be accelerated by centripetal forces to several times the Kepler speed at the injection point. Given that most YSO jets have speeds of $\sim 10^2$ km s^{-1}, much of the material in this component must originate within ~1 AU of the YSO. However, slower winds can be launched from larger radii. The visual wavelength forbidden [OI] lines (Natta et al. 2014) and multiple absorption components of NaI and Ca H and K toward some TTauri stars (Mundt 1984, Hartigan et al. 1995, Pascucci et al. 2015) and Herbig AeBe stars (Waters & Waelkens 1998) provide evidence for a range of ejection velocities. The densest gas associated with the collimated jets tends to have the highest speeds, whereas the lower-density material may trace slower winds from a disk (Wardle & Koenigl 1993). Additionally, the swept-back appearance and increasing excitation conditions in the wings of the jet-powered internal working surfaces associated with jet knots indicate the presence of a lower-density, slower component surrounding the jets. HST images of HH 34 (Reipurth et al. 2002), HH 47 (Heathcote et al. 1996), and HH 111 (Reipurth et al. 1997b) provide examples. Thus, both X-winds and disk winds may be present in YSOs.

Although the primary winds are accelerated within a few astronomical units of the source stars, observations and theory suggest that collimation occurs on scales of tens to hundreds of astronomical units from the acceleration site. Cantó & Rodriguéz (1980) presented a purely HD collimation mechanism in which density gradients in the envelope surrounding the forming star created a nozzle-shaped cavity that redirects a diverging flow into a converging one. Crossing shocks in the convergence zone dissipate and thermalize the converging component of the flow but preserve the component away from the source, resulting in the formation of a downstream jet. Although there may be few examples of Cantó nozzles, such as HH 39 from R Mon in

NGC 2261 (Cantó et al. 1981), the outflow from XZ Tau in L1551, and HH 626 in Orion, most research has concentrated on collimation produced by the hoop stress of toroidal magnetic fields. The collimation region in some YSOs can be traced by stationary X-ray emission a few hundred astronomical units from the source star (Schneider et al. 2011). Models show that X-ray emission can be formed in wind-wind collisions, in which a slower wind, possibly from the disk, interacts with a faster wind emerging from a region closer to the YSO (Günther et al. 2014).

X-wind and disk-wind models predict that the mass ejection rate should be comparable with the mass accretion rate (Shu et al. 1988, 1991). Ellerbroek et al. (2013) compiled measurements of mass loss and accretion rates for a collection of YSOs in various evolutionary stages with different masses. The results, shown in **Figure 4**, indicate that the mean mass-loss rate in protostellar jets is given by $\dot{M}_{\rm jet} \sim 0.1\dot{M}_{\rm acc}$. However, the observations only trace the relatively dense component in collimated jets that may be surrounded by wider-angle flows with lower density.

Both X-winds and disk winds are expected to launch rotating winds. However, because the nearest jets are at distances of ~100 pc and the best angular resolution currently available is about 0.1 arcsec, measurements of jet rotation are difficult. Interpretation of the data can be complicated by interactions of the jet with the environment, which can produce velocity gradients. Nevertheless, there are some convincing measurements of jet rotation with speeds of a few km s^{-1} (Cabrit 2007, Ray et al. 2007, Frank et al. 2014, Zapata et al. 2015).

3. OUTFLOWS FROM CLUSTERS AND MASSIVE STARS

Most stars form in compact, short-lived clusters or small groups of stars in nonhierarchical systems (Lada & Lada 2003). Clusters of YSOs power clusters of outflows. The entire Perseus cloud has been surveyed for HH objects (Walawender et al. 2005a,b, 2006) and molecular outflows (Hatchell & Dunham 2009; Arce et al. 2010, 2011); major centers of outflow activity in decreasing order of richness are NGC 1333, the southwest portion of the IC348 cluster containing HH 211, the Barnard 1 region, L1448, and L1455, followed by a relatively distributed population of outflows.

Figure 10 shows NGC 1333 at visual to near-IR wavelengths. The cluster contains over 140 low-mass YSOs with the most massive member being spectral type B5 (Lada et al. 1996, Hatchell et al. 2013). Several dozen outflows produce a profusion of HH objects (Bally et al. 1996), MHOs, and overlapping molecular outflow lobes (Hatchell & Dunham 2009, Curtis et al. 2010, Bieging et al. 2014). Only a few jets are visible; most of the shocks exhibit complex and chaotic structure. Several outflows have HH extensions parsecs beyond the confines of the molecular cloud (Walawender et al. 2005b). **Figure 11** shows a CO map of the central 7-arcmin-by-7-arcmin region (Plunkett et al. 2013). NGC 1333 is pockmarked with cavities that Quillen et al. (2005) and Bieging et al. (2014) proposed were carved by a previous generation of outflows. Maret et al. (2009) used *Spitzer*/IRS to map the S(0) to S(7) lines in the pure rotational spectrum of H_2. These lines originate in 12–53-km s^{-1} C-type shock. The total H_2 luminosity is estimated to be 0.25 to 0.5 times the mechanical luminosity of the driving outflows. These authors found that feedback can be the main mechanism for core disruption but may not disrupt the entire cloud.

The number of known flows in NGC 1333 is at least a factor of four less than the number of identified YSOs. The duration of the prominent phase of outflow activity as traced by CO, MHOs, or HH objects is linked to the duration of active accretion and is shorter than the duration of star formation in the cluster, which is thought to be at least 2 to 5 Myr from stellar age spreads. A main outflow lifetime of 0.5 Myr is consistent with the estimated duration of the Class 0 and I phases of YSO evolution (Evans et al. 2009). It is also possible that some stars do not power prominent outflows. If the outflow is poorly collimated, has a wide-opening angle, or emerges as a wide-angle wind, the density may fall off too rapidly to produce detectable shocks. It is also possible that the

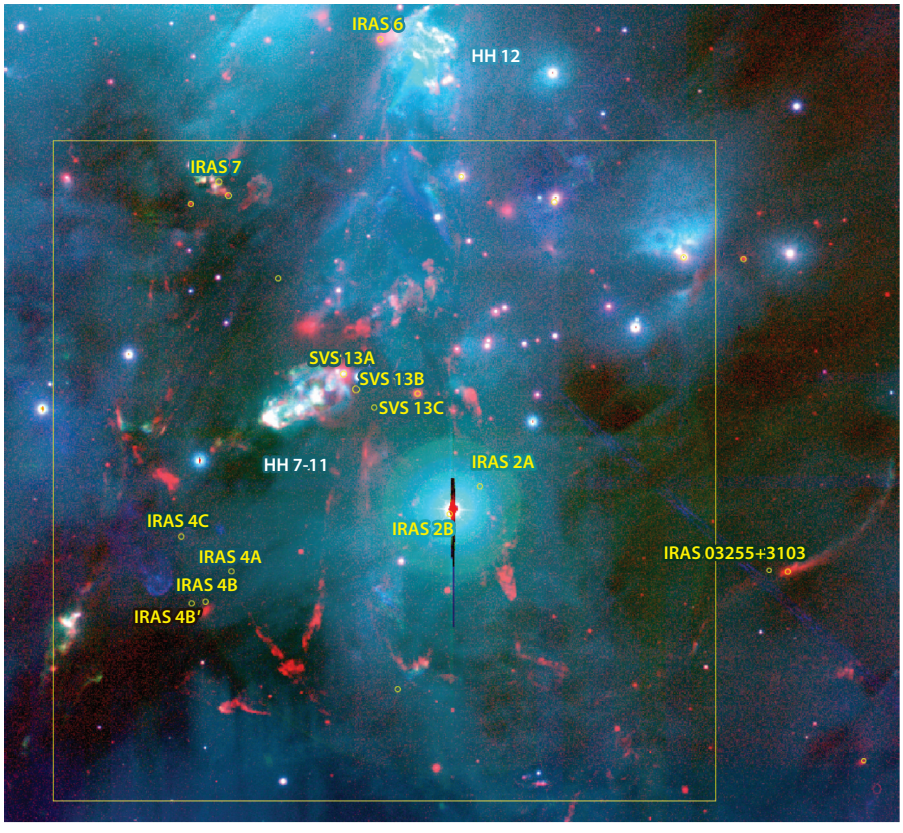

Figure 10

An Hα (*blue*), [SII] (*green*), and H_2 (*red*) image showing the core of the NGC 1333 cluster. The yellow box shows the 8-arcmin-by-8-arcmin field of view shown in **Figure 11**. HH 7–11, HH 12, and the S-symmetric outflow from IRAS 03256+3055 are marked. The 138-$L_\odot$ binary SVS3 (spectral type B5 + F2) illuminates the NGC 1333 reflection nebulosity above the top edge of the image and dominates radiative feedback in NGC 1333 (Hatchell et al. 2013). IRAS 03255-3103 near the right edge drives an S-symmetric outflow. Small yellow circles mark radio sources identified by Tobin et al. (2015). The Hα and [SII] images were obtained by Bo Reipurth with *Subaru* (unpublished); the H_2 image was obtained by Josh Walawender with WFCAM on UKIRT (unpublished).

most powerful outflows require triggering by large accretion events. Reipurth (2000) proposed that interactions with sibling stars in multiple systems and disintegrating nonhierarchical stellar groups perturb disks and envelopes and trigger major accretion events that produce powerful outflows.

There are many other known clusters of outflows from forming stellar groups including IC 348SW (Arce et al. 2010), ρ-Oph (Nakamura et al. 2011), Serpens-Main and South (Plunkett et al. 2015), L1641N (Nakamura et al. 2012), L1551 (Stojimirović et al. 2006), B59 (Duarte-Cabral et al. 2012), IRAS 05358+3543 (Ginsburg et al. 2009), and the Gulf-of-Mexico region of the North America and Pelican Nebula complex (Armond et al. 2011, Bally et al. 2014). The Orion B cloud contains the NGC 2071 cluster (Stojimirović et al. 2008). Orion A is full of MHOs (Davis et al. 2009). The integral shaped filament in the Orion A cloud contains over 2,000 YSOs and dozens of molecular outflows, irradiated jets inside the Orion Nebula, and parsec-scale flows blowing clear of the molecular cloud (Yu et al. 1997, 2000; Williams et al. 2003; Takahashi et al. 2008).

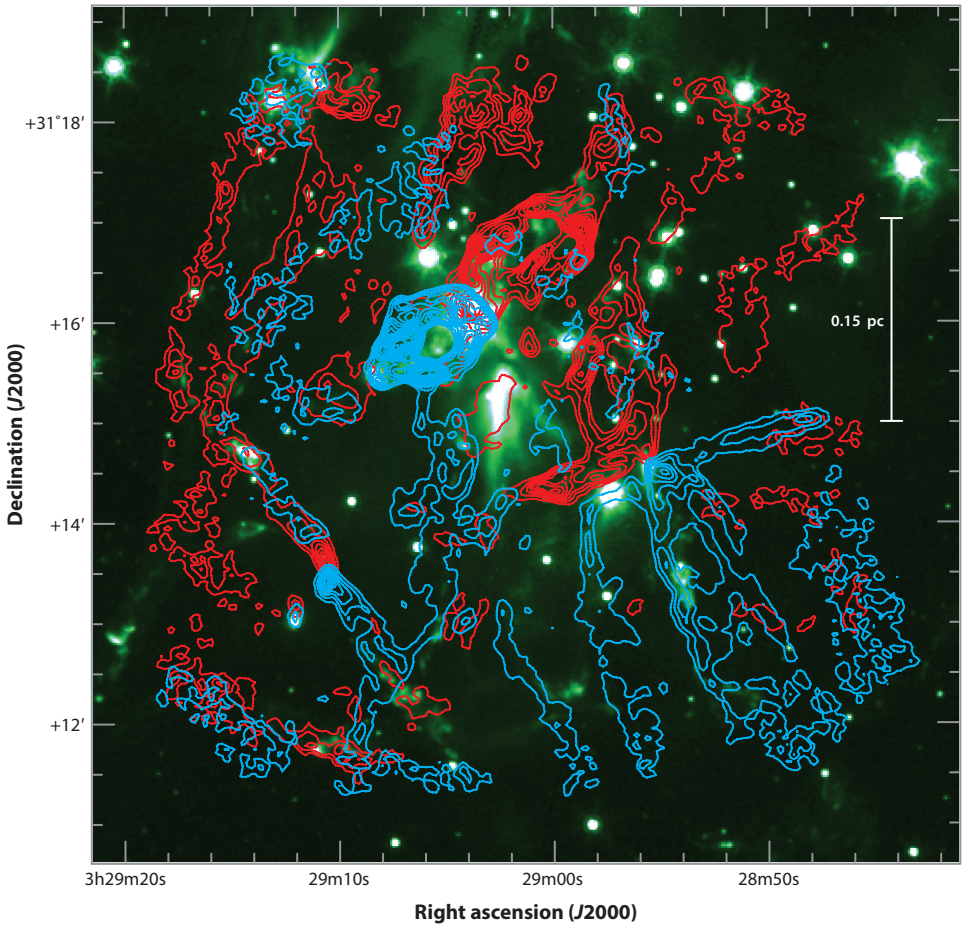

Figure 11

A CO $J = 1$–0 map showing multiple outflows in an 8-arcmin-by-8-arcmin (0.5 pc) field in NGC 1333 with 5-arcsec (1,000 AU) angular resolution. Red and blue contours show red-shifted and blue-shifted outflow lobes superimposed on a *Spitzer*/IRAC 4.5 μm image (*green*). The data taken with the Combined Array for Research in Millimeter-wave Astronomy interferometer only covers the central 7-arcmin-by-7-arcmin field of the 8-arcmin-by-8-arcmin field shown (Plunkett et al. 2013).

The Orion Nebula contains dozens of supersonic outflows traced by fully ionized shocks whose proper motions reveal their presence (O'Dell et al. 2015). OMC1-S, located about 90 arcsec south of OMC1, contains several dozen highly embedded YSOs that power over a half-dozen outflows, some of which protrude into the Orion Nebula (Zapata et al. 2004a,b, 2005, 2006; Henney et al. 2007).

Low-mass stars: stars in the range of $0.08 < M < 2$ $M_\odot$

High-mass stars: stars with $M > 8$ $M_\odot$

Intermediate-mass stars: stars with $2 < M < 8$ $M_\odot$

3.1. Outflows from High-Mass Young Stellar Objects

In the 1980s and 1990s, research concentrated on the study of nearby outflows from low-mass stars. With the advent of millimeterwave interferometers, IR arrays, and IR and submillimeter space missions, the more distant, highly obscured, and relatively rare intermediate- and high-mass YSOs and massive star clusters have received increased attention. Do massive stars form

THE BN/KL OUTFLOW FROM OMC1 BEHIND THE ORION NEBULA

The Orion Nebula (O'Dell 2001) and the molecular cloud located behind the Nebula played pivotal roles in our understanding of outflow phenomena and their relation to star formation. Becklin & Neugebauer (1967) discovered a luminous but obscured IR star, the BN object, ∼1 arcmin from the Trapezium stars that ionize the Nebula. Kleinmann & Low (1967) discovered an IR nebula about 10 arcsec south of BN. Thus, the complex containing BN and this nebula is known as the BN/KL region. BN is a runaway star moving toward the northwest at about 24 km s^{-1} in the rest-frame of the Nebula stars (Plambeck et al. 1995, Gómez et al. 2008). Chatterjee & Tan (2012) suggest that BN was ejected from the Trapezium about 5,000 years ago. However, radio source I (Menten & Reid 1995), thought to be another massive star embedded in BN/KL, is moving with a speed of ∼15 km s^{-1} in a direction opposite to BN. BN/KL has a luminosity of about 10^5 $L_\odot$ and is embedded in a ∼100 $M_\odot$ dense and hot cloud core known as Orion Molecular Core 1 (OMC1), the densest and most molecule-rich part of the 50,000 $M_\odot$ Orion A molecular cloud that gave birth to the Nebula (Genzel & Stutzki 1989). The presence of an energetic outflow in OMC1 was recognized by Kwan & Scoville (1976) and Zuckerman et al. (1976). Observations of the Orion region have continued to produce new discoveries and insights; De Buizer et al. (2012) recently found that IRc4, located ∼6 arcsec southwest of source I, may also contain a 20,000 $L_\odot$ protostar.

like low-mass ones, or is there additional physics involved? The morphology of many outflows from MYSOs appears to be similar to that from low-mass YSOs. Jets and EHV and SHV shells are also seen in intermediate-mass YSOs such as IRAS 20050+2720 (Bachiller et al. 1995) and clusters containing MYSOs such as DR21 and G331.512−0.103 (Qiu & Zhang 2009; Zapata et al. 2009b, 2011, 2013b; Merello et al. 2013). Some luminous sources such as the 1.7×10^4-$L_\odot$ IRAS 18162-2048 (HH 80/81) power fast jets and giant outflows. The most massive member of this small cluster drives a $>10^3$-km s^{-1} radio jet (Martí et al. 1998) that energizes the high-excitation shock complex HH 80/81 and powers giant outflow 18.4 pc in length (Masqué et al. 2012, 2015; Fernández-López et al. 2013).

3.2. An Example: Orion BN/KL

Orion contains the nearest forming massive stars (see the sidebar The BN/KL Outflow from OMC1 Behind the Orion Nebula). The BN/KL region behind the Orion Nebula, located at a distance of ∼414 pc (Menten et al. 2007), contains a powerful, wide opening–angle, arcminute-scale outflow emerging from the OMC1 cloud core traced by millimeter and submillimeter emission lines of CO, CS, SO, SO_2, and HCN that exhibit broad (>100 km s^{-1}) emission line wings (Kwan & Scoville 1976, Wiseman & Ho 1996, Furuya & Shinnaga 2009); high-velocity OH, H_2O, and SiO maser emission (Greenhill et al. 1998); and bright shock-excited "fingers" of H_2 and "fingertips" of 1.64-μm [FeII] emission (Allen & Burton 1993; Lee & Burton 2000, Colgan et al. 2007; Nissen et al. 2007; Bally et al. 2011, 2015). The Orion OMC1 BN/KL outflow exhibits hundreds of individual bow shocks in the near-IR lines of H_2 and [FeII], some of which exhibit proper motions of over 300 km s^{-1} (see **Figure 12**; Bally et al. 2011, 2015). The CO emission exhibits a cluster of molecular streamers emerging from between the BN and source I: two massive protostars embedded in the Orion OMC1 cloud core that were ejected in opposite directions about 500 years ago (Zapata et al. 2009c, 2011; Peng et al. 2012).

The BN/KL outflow contains at least 8 $M_\odot$ of accelerated gas with a median velocity of about 20 km s^{-1}. Interferometric CO images, H_2O and the 18-km s^{-1} SiO masers, and dense-gas tracers such as thermal SiO emission reveal a smaller, 8 arcsec (0.016 pc)-long and younger

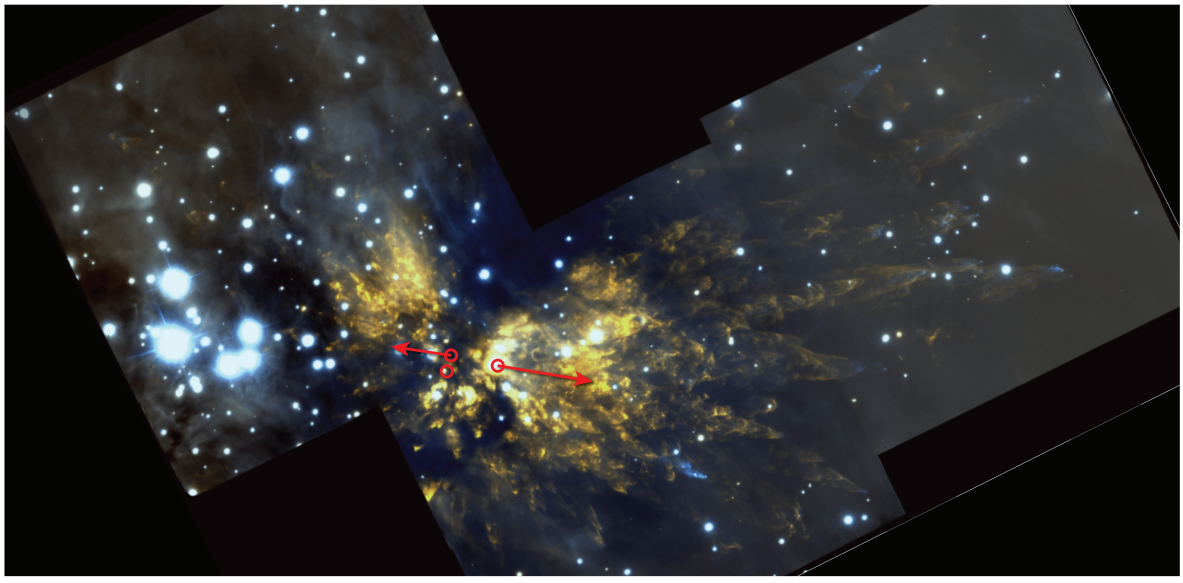

Figure 12

Image showing the OMC1 outflow in the 2.122-μm H_2 line (*orange*) and 1.644-μm [FeII] lines with locations of the BN object, source I, and n indicated by red circles. The red vectors show the 21.6-km s^{-1} proper motion of BN toward position angle (PA) = 331° (*right*) and the 14.6-km s^{-1} proper motion of source I toward PA = 142° (*left*) measured by Gómez et al. (2008). Goddi et al. (2011) measured slightly different proper motions of 26.4 km s^{-1} toward PA = 341° for source I and 11.5 km s^{-1} toward PA = 109°. BN has a redshift of +11 km s^{-1}, whereas source I has a blueshift of −4 km s^{-1} with respect to the V_{LSR} = 9-km s^{-1} radial velocity of OMC1. Recently, Rodriguez and colleagues (in preparation) found that source n is also moving toward the PA = 192° with a velocity of about 45 km s^{-1}, which is somewhat higher than the 26-km s^{-1} motion toward PA = 180° found by Gómez et al. (2008). These motions are in the Orion reference frame. The lengths of the vectors are equal to the motion in 2,000 years (e.g., 10 arcsec corresponds to a motion of ∼10 km s^{-1}). Adapted from J. Bally, Ginsburg A, Arce H, Eisner J, et al. (in preparation).

(<200-year-old) outflow along a northeast-southwest axis emerging from radio source I, orthogonal to the arcminute-sized CO outflow (Beuther & Nissen 2008, Plambeck et al. 2009). The momentum and kinetic energy content of these flows is at least 160 $M_\odot$ km s^{-1} and 4×10^{46} ergs (Snell et al. 1984) to 4×10^{47} ergs (Kwan & Scoville 1976). Zapata et al. (2009c) presented a CO $J = 2$–1 interferometric study and found a dynamic age of ∼500 years for the larger OMC1 outflow, implying a momentum injection rate $\dot{P} \sim 0.3$ $M_\odot$ km s^{-1} $year^{-1}$. They noted its explosive nature, which differs from jets and collimated bipolar outflows, and that it originated several arcseconds north of the OMC1 hot core. **Figure 13** shows an ALMA image of the $J = 2$–1 CO emission. Though early single-dish maps hinted at some bipolarity (Erickson et al. 1982), the ALMA images show that the flow is nearly isotropic with over 100-arcsec-wide CO streamers exhibiting linear velocity gradients with $V \propto D$, where D is the distance from the suspected explosion center. These velocity gradients indicate a dynamic age of ∼500 years.

The motion of BN and radio source I away from a region less than 500 AU in diameter from which they were ejected about 500 years ago has been confirmed by a number of groups (Rodríguez et al. 2005; Gómez et al. 2005, 2008; Goddi et al. 2011). The BN object is a 12- to 15-$M_\odot$ MYSO (Scoville et al. 1983, Rodríguez et al. 2009). Momentum conservation implies that source I, which was ejected from OMC1 with about half the velocity of BN, must have a mass of $\sim 22 \pm 3$ $M_\odot$.

Bally & Zinnecker (2005) proposed that the BN/KL explosion may have been triggered by a stellar merger or the dynamical rearrangement of a nonhierarchical system of massive stars into a

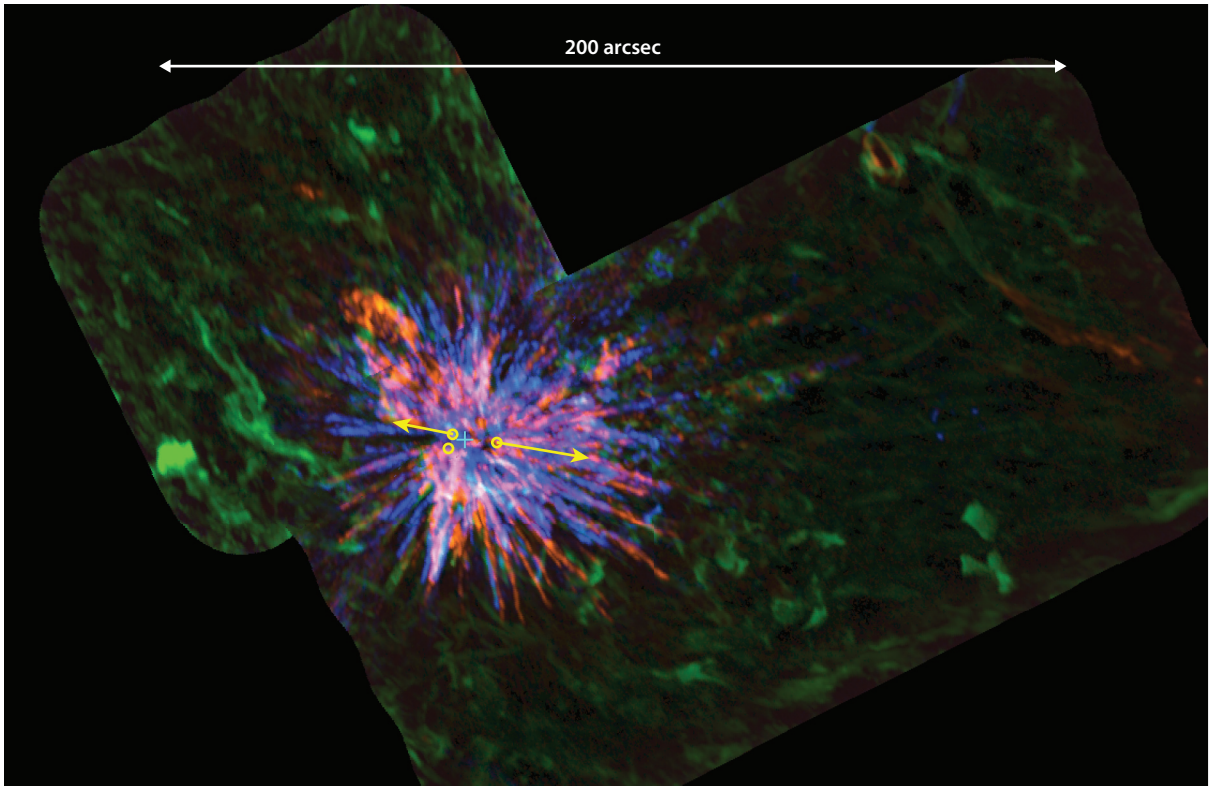

Figure 13

An ALMA 1.3-mm image showing the 230-GHz CO $J = 2$–1 emission from the explosive BN/KL outflow with 1 arcsec (~450 AU) angular resolution. Blue-shifted emission from $V_{LSR} = -110$ to 0 km s^{-1} is shown in blue, red-shifted emission from $V_{LSR} = +20$ to $+130$ km s^{-1} in red, and the emission from $V_{LSR} = 0$ to $+20$ km s^{-1} around the rest velocity of the OMC1 core is shown in green. Only the small-scale structure in the cloud is shown by the green channel because of the spatial filtering effect of the ALMA interferometer. The yellow arrows show the motions of the BN object and source I as in **Figure 12**. This image is shown in Galactic coordinates. Adapted from Bally et al. (2015) with permission.

hierarchical system that resulted in their ejection from the OMC1 core as high-velocity, runaway stars. In this model, the disruption and ejection of circumstellar disks and envelopes produced the BN/KL outflow. The momentum and kinetic energy of the outflow and ejected stars came from the release of gravitational binding energy of a compact binary formed by the dynamic interaction of three or more stars.

Zapata et al. (2009c), Bally et al. (2011), and Goddi et al. (2011) found supporting evidence for the dynamical rearrangement model. In this scenario, the final N-body encounter would have resulted in the formation of a compact, astronomical unit–scale binary, or possibly a protostellar merger, most likely source I, and the ejection of source I and BN. However, it is still possible that additional highly embedded IR sources will be found in dense cores such as the 1-mm source SMA1 (Beuther & Nissen 2008). De Buizer et al. (2012) found that the source IRc4, located 6 arcsec southwest of source I, may harbor an MYSO with $L \sim 2 \times 10^4$ L$_\odot$. Radio source I has not yet been directly detected at any IR wavelength. However, source I illuminates an IR reflection nebula about 10 arcsec to the east, and its spectrum indicates an effective photospheric temperature of ~4,000 K similar to a K or M supergiant (Morino et al. 1998, Testi et al. 2010).

Hosokawa & Omukai (2009) and Hosokawa et al. (2010) show that MYSOs accreting at high rates develop bloated photospheres and cool photospheric temperatures. For accretion rates $\dot{M} > 10^{-3}$ $M_\odot$ year^{-1}, photospheric radii can exceed 1 AU. If the BN/KL dynamic interaction resulted in a member of OMC1 passing within ~1 AU of a rapidly accreting MYSO, it would have entered the massive star's photosphere, possibly triggering a stellar merger. The sudden release of gravitational potential energy would have produced the explosion. The interaction of the ejecta with the surrounding cloud core could have resulted in mass sorting of the ejecta, which upon emergence from the core could produce the observed CO fingers, H_2 wakes, and [FeII] bullets.

Orion may not be unique. *Spitzer* detected 4.5-μm emission from a wide-angle outflow having a morphology similar to Orion emerging from a high-luminosity (~10^6-$L_\odot$) hot core in G34.25+0.16 in the inner Galaxy (Cyganowski et al. 2008). Unfortunately, this flow and its source are at a distance of ~5 kpc and highly obscured. The HH 105 outflow in the NGC 7129 star-forming region has a morphology suggestive of an explosive origin in the *Spitzer* 4.5-μm images (Eislöffel 2000, Morris et al. 2004). This flow originates from a moderate luminosity (<10^3-$L_\odot$) protostar LkHα234. Source G in W49, the most luminous water maser outflow in the Milky Way, may be another example (Smith et al. 2009). Sahai et al. (2008) found evidence for interstellar bullets similar to the OMC1 fingers in the outflow from the massive young protostar IRAS 05506+2414.

3.3. Outflows from Massive Young Stellar Objects

There has been intense debate within the star-formation community about massive star formation. Do MYSOs form in a scaled-up version of low-mass star formation, or is there additional physics such as interactions with sibling stars, radiation pressure, and ionization involved? Most massive stars form in clusters and tend to have short pre-main-sequence phases; as they grow past 10 $M_\odot$, some continue to accrete despite being on the main-sequence with high-UV luminosities (Keto 2003). Reipurth (2000) and Reipurth & Mikkola (2012) emphasized the role of N-body interactions in determining the mass-spectrum of forming YSOs and in the production of outflows. Such interactions may be even more important in massive star formation because MYSOs tend to form in dense groups and clusters.

Massive stars drive faster and more powerful outflows than lower-mass stars. Yet they do not appear to be larger or longer than flows from lower-mass YSOs. In part this may be because of the higher density of massive star-forming environments, more rapid evolution of MYSOs, the destruction of outflow signatures by feedback from other cluster members, or observational selection effects related to their larger distance and higher extinction.

Although most outflows from high-mass YSOs appear to be collimated, many exhibit complex structure. Some MYSOs power radio jets with high proper motions. Cepheus A ($D \sim 700$ pc, $L \approx 2 \times 10^4$ $L_\odot$) contains a pulsed, precessing jet and a complex CO outflow (Zapata et al. 2013a). Near the source, the radio jet exhibits ~500-km s^{-1} proper motions (Curiel et al. 2006, Jiménez-Serra et al. 2011, Torrelles et al. 2011). Cunningham et al. (2009) proposed that the disk around the 15-$M_\odot$ primary experiences forced precession driven by a companion in an eccentric, noncoplanar orbit. During periastron passages, the companion perturbs the disk and triggers accretion and episodes of jet production. IRAS 16547-4247 ($D \sim 2.9$ kpc, $L \approx 6 \times 10^4$ $L_\odot$) is embedded in a 1,300-$M_\odot$ clump and powers an antisymmetric S-shaped thermal radio jet with proper motions of ~490 km s^{-1} (Rodríguez et al. 2005, 2008) that may power a molecular outflow with $M \approx 110$ $M_\odot$ and $V \approx 120$ km s^{-1} (Garay et al. 2003, 2007; Higuchi et al. 2015); it is possibly powered by several sources in a forming cluster of stars. G35.20−0.74N ($D \sim 2.2$ kpc, $L \sim 1$–10×10^4 $L_\odot$) contains a compact, 0.15 by 0.13 pc, ~130-$M_\odot$ "necklace" of dense cores

sounding the waist of a mid-IR bipolar nebula (Sánchez-Monge et al. 2014). A wide-angle bipolar molecular outflow and a complex MHO may be powered by several MYSOs including a precessing radio jet emerging from one of the cores. Klaassen & Wilson (2007, 2008) presented a survey of SiO and HCO^+ toward 23 massive star-forming regions containing ultra-compact HII regions and detected SiO toward about half. The presence of powerful outflows and HII regions indicates ongoing accretion despite the presence of ionization feedback. However, line-of-sight confusion may alter the interpretation. There may be older YSOs destroying their natal environment while, nearby, embedded MYSOs are still accreting. The Orion Nebula and adjacent BN/KL region present a similar situation.

The W51 complex ($D \sim 5.5$ kpc) is one of the most luminous in the Galaxy (Zapata et al. 2009a, Ginsburg et al. 2015). Lacy et al. (2007) found a remarkable ionized jet near the 2–4 $\times 10^6$-$L_\odot$ IR source and nascent massive star cluster W51 IRS 2, which has a Lyman continuum luminosity of nearly 10^{50} photons s^{-1}, nearly 50 times the Orion Nebula. With a radial velocity of $\sim$100 km s^{-1} in the 12.8-μm [NeII] and 10.5-μm [SIV] lines, the jet has an ionized mass of $\sim 3 \times 10^{-3}$ $M_\odot$ and a mass-loss rate of $\dot{M} > 1.2 \times 10^{-5}$ $M_\odot$ $year^{-1}$; it is one of the few protostellar outflows bright in radio recombination lines. Zapata et al. (2009a) found a $\sim$200-$M_\odot$ bipolar molecular outflow in the same region but emerging at nearly right angles to the [NeII] jet. The molecular outflow with $\dot{P} \sim 3$ $M_\odot$ km s^{-1} $year^{-1}$ emerges from an $\sim$60-$M_\odot$ proto-O star surrounded by an $\sim$40-$M_\odot$, 9,000-AU-diameter, ring-shaped envelope.

Van Kempen et al. (2015) studied six intermediate-mass star-forming regions to evaluate relationships between the outflow momentum injection rate and the luminosity of massive stars and found that the trends identified for low-mass YSOs extend smoothly through the intermediate YSO regime into the MYSO regime. Caratti o Garatti et al. (2015) conducted a survey of near-IR H_2 emission toward luminous, $L > 5 \times 10^3$ $L_\odot$, star-forming complexes thought to be forming MYSOs with $M > 8$ $M_\odot$ and identified as EGOs (Cyganowski et al. 2008; Chen et al. 2013a,b). Caratti o Garatti et al. (2015) found a correlation between the total H_2 and bolometric luminosity of the source star or cluster, $L(H_2) \sim 0.03 L_{\rm bol}^{0.6}$ $L_\odot$. Duarte-Cabral et al. (2013) analyzed the properties of outflows from highly embedded MYSOs in the Cygnus-X region. Maud et al. (2015a) presented a comprehensive study of a distance-limited sample of 99 massive star-forming clumps selected from the Red MSX Source survey with luminosities ranging from 10^3 to 10^6 $L_\odot$ and clump masses ranging from 10 $M_\odot$ to nearly 10^4 $M_\odot$. Maud et al. (2015b) investigated the molecular outflows from these sources. **Figure 14** shows the estimated momentum injection rate as a function of source luminosity for a collection of outflows from YSOs and MYSOs. Because mass estimates are usually based on a single transition, which is insensitive to hot and nonmolecular components, the mass momentum injection rates into the surrounding cloud are likely lower limits. The most active outflows are associated with the main accretion phases of forming stars. Fitting the dotted line in **Figure 14** implies that the molecular outflow momentum injection rates from low-mass Class 0 sources through massive accreting protostars scale as $\dot{P}_{\rm out} \approx 2 \times 10^{-5} L^{0.6}$ $M_\odot$ km s^{-1} $year^{-1}$, where L is the luminosity in $L_\odot$. Assuming that most pre-main-sequence luminosity comes from accretion on the birth-line and scales roughly as $L \propto M_1^2$ with stellar mass M_1 in units of 1 $M_\odot$, this can be recast as $\dot{P}_{\rm out} \approx 1.25 \times 10^{-4} M_1^{1.2}$, where we use the mean luminosity $L \approx 20$ $L_\odot$ of a 1-$M_\odot$ star descending from the birth-line during its main accretion phase for the normalization.

Forming massive stars and star clusters may power high-mass outflows by using the thermal expansion of photoionized plasma as a drive. The massive, 3,000-$M_\odot$, parsec-scale, bipolar outflow emerging from DR 21 in Cygnus (Russell et al. 1992, Zapata et al. 2013b) may be powered by the acceleration of plasma confined by the surrounding dense cloud. The flow emerges at right angles to a molecular filament that spawned a cluster of a dozen or so OB stars in the center of

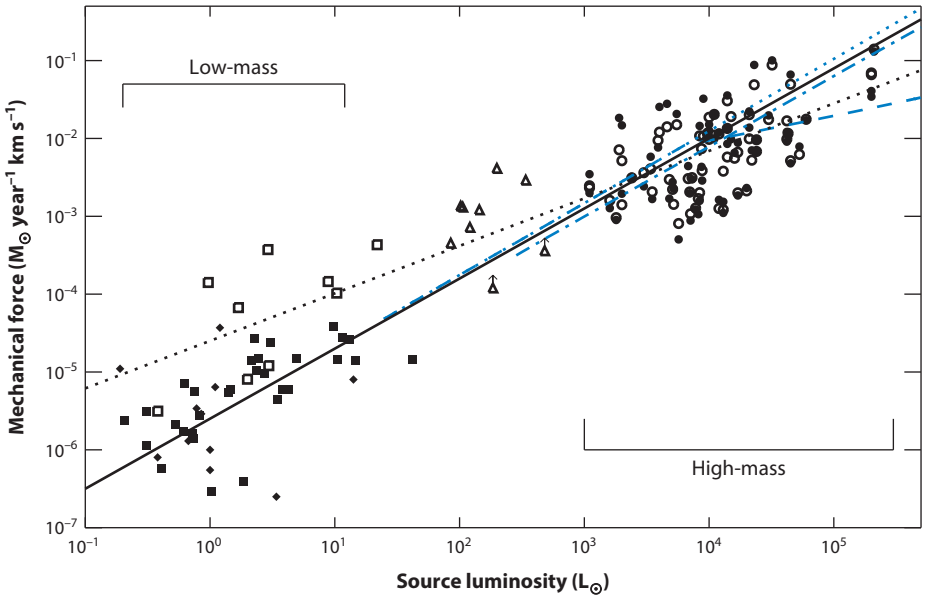

Figure 14

The momentum injection rate or force exerted by outflows from star-forming clumps as a function of the clump luminosity for a distance-limited sample with $D < 6$ kpc based on CO $J = 3$–2 data. The filled and open circles represent the massive young stellar object (MSYO) sample of Maud et al. (2015b) using two methods for estimating the outflow age described in the text. The open and filled squares are low-mass Class 0 and Class I outflow sources from Bontemps et al. (1996); the filled diamonds are from van der Marel et al. (2013); the open triangles are MYSOs from Duarte-Cabral et al. (2013). The solid black line shows the trend for Class I sources from Bontemps et al. (1996). Taken from Maud et al. (2015b).

the flow. The DR 21 outflow is one of the few that has been imaged in the 21-cm HI line. Russell et al. (1992) proposed that photoionization of the dense molecular filament from which the O stars formed drives a champagne flow that accelerates to several times the sound-speed in photoionized gas and then recombines because of the ongoing resupply of plasma by the photoablation of the dense gas. Such a model works only if the morphology of the dense gas can confine the thermal expansion of the plasma. To demonstrate the physics, consider the plasma flows induced by a source of ionization in a long, hollow cylinder or tube of dense gas much denser than Strömgren density at the radius of the hollow region.

There is evidence for powerful bipolar ejections during the main-sequence evolution of some massive stars. The giant ionized bipolar outflow Ou4 in the HII region Sh-2-129 has a length of ∼15 pc, a kinetic energy of about 4×10^{47} ergs, and a dynamic age of about 90,000 years (Corradi et al. 2014). The bipolar flow is bright in [OIII], which exhibits radial velocities of order 100 km s^{-1} with respect to the surrounding HII region and is collisionally ionized. Ou4 was apparently produced by the main-sequence triple system HR 8119 consisting of two B0 V stars and one B0.5 V star. A parsec-scale bubble of warm dust centered on HR 8119 may indicate a recent cataclysmic event in this multiple-star system, such as a dynamic interaction or possibly a stellar merger. However, it is possible that fast, ∼2,000 km s^{-1}, stellar winds with a combined mass-loss rate of 4×10^{-8} $M_\odot$ year^{-1} could also power the bubble. The collimated nature of Ou4 is highly unusual for a stellar wind and requires the existence of a collimation mechanism.

The transition from protostellar outflows during stellar birth to main-sequence stellar winds is poorly understood. Although most MYSOs produce collimated outflows during their formation, possibly punctuated by short-duration violent eruptive phenomena such as the Orion BN/KL outflow, main-sequence stellar winds appear to be isotropic. Protostellar outflows are rendered visible by interactions with their surroundings and by internal working surfaces formed in velocity-variable flows. As the parent environment is dispersed, these interactions, combined with declining outflow activity, become increasingly difficult to detect. Many MYSOs exhibit $\Delta V \sim$ 100–500-km s^{-1} wide near-IR hydrogen recombination lines indicating dense, ionized winds (Simon et al. 1983, Jaffe & Martín-Pintado 1999, Lumsden et al. 2012). These signatures disappear as stars reach the main sequence and develop faster winds. Emission in UV-resonance lines and absorption from ground-state transitions are the main tools for their detection. Observations of the transition from protostellar outflow to main-sequence stellar winds remain a challenge.

4. THE ROLE OF OUTFLOWS IN FEEDBACK AND SELF-REGULATION

Two scenarios have been proposed for the way feedback can impact clustered star formation: rapid cloud dispersal in a few turbulent velocity crossing times following a burst of star formation (Elmegreen 2007, Hartmann & Burkert 2007) and slow, quasi-equilibrium star formation regulated by the replenishment of turbulence by feedback (Tan et al. 2006, Nakamura & Li 2007, 2014). The injection of momentum and energy, by protostellar jets, bipolar outflows, and wide-angle winds, and of soft-UV, from moderate-mass stars, ionizing radiation, stellar winds, and explosions of massive stars, can drive shocks that dissociate and heat the gas, generate turbulence, and disperse the material. Although cluster-forming clumps such as NGC 1333, Serpens South, and Ophiuchus (all with $M \sim 500$ M$_\odot$, R ~ 0.5 pc) may have shorter lifetimes, the duration of star formation in most GMCs such as Orion ($M \sim 10^5$ M$_\odot$, R ~ 50 pc) is comparable with the main-sequence lifetimes of massive stars, ~5 to 15 Myr. Thus, feedback by all of these mechanisms impacts the ecology of star-forming regions (Krumholz et al. 2011, Myers et al. 2014). As stars gain mass from their host cores, protostellar outflows form the first rung of a feedback ladder of ever more powerful energy and momentum injection mechanisms.

Outflow feedback in low-mass, weakly bound clouds that are only forming a few to a few dozen stars can generate turbulence, limit the collapse rate, and disrupt the parent clouds (Matzner 2007, Matzner & Jumper 2015). In isolated small clouds, or filaments such as Taurus, outflows tend to blow out of their parent cores, making feedback less efficient. Nevertheless, in small clouds such as L1551, outflows from a half-dozen embedded YSOs have created swept-up CO lobes and HH objects covering about 30% of the projected area of the cloud (Stojimirović et al. 2006). As flows age, their cavities widen, and a large portion of the host clump can be impacted (Matzner & McKee 1999). In more massive cluster-forming clumps such as NGC 1333 and L1641N, outflows appear capable of maintaining turbulence and therefore limiting the rate of star formation (Arce et al. 2010, Nakamura et al. 2012, Bally et al. 2014). However, outflow activity has not brought star formation to a halt. Drabek-Maunder et al. (2015) used CO $J = 3$–2 to analyze the impact of outflow momentum and energy injection in the nearby Serpens Main, Ophiuchus, and Perseus clouds, concluding that outflows account for at least 20% of the turbulent energy in these clouds. Nakamura & Li (2007) and Federrath et al. (2014) modeled turbulence generation in clouds by clusters of outflows; Nakamura & Li (2011) explored the role of magnetic fields in such environments, finding that outflows are more important. In these clusters, shocks traced by HH objects and MHOs cover a large fraction of the projected cloud surface area. Assuming an area covering factor of shocks, f_A (e.g., **Figure 10**), a random orientation of outflows, and a mean shock velocity V_s, the timescale in which half of the cloud is reprocessed by shocks is $t \sim t_{cross}/f_A = R_{cloud}/V_s f_A \sim 10^5$ years for $R_{cloud} = 1$ pc, $V_s = 100$ km s^{-1}, and $f_A = 0.1$.

Carroll et al. (2009) predicted a change in the slope of outflow-driven turbulence on the scale of a typical flow, adopting ~0.3 pc for this parameter. Padoan et al. (2009) used the power spectrum of turbulence in the NGC 1333 region of the Perseus cloud to argue that outflows were unlikely to drive turbulence because of the absence of a flattening in the turbulent energy spectrum above the expected outflow injection scale. However, these studies failed to properly account for the observed sizes of giant outflows that can inject momentum and drive turbulence on scales up to tens of parsecs. There may not be a clear break in the scale of turbulence driving by outflow feedback.

Nakamura & Li (2014) presented an analytic model for outflow feedback, comparing momentum and energy injection rates with turbulence dissipation rates. The analytic approximations are compared with observations of eight cluster-forming clumps with masses ranging from 30 to 1,100 $M_\odot$. They found that the outflow momentum injection rate, $\dot{P}_{\rm out}$, of outflows resulting from a star-formation rate of a few percent per free-fall time is sufficient to balance the turbulent dissipation rate. For the lowest-mass clumps B59, L1551, and L1641N, $\dot{P}_{\rm out}$ is about ten times larger than the turbulent dissipation rate, $\dot{P}_{\rm turb}$. The outflows maintain turbulent motions with an amplitude five to ten times the sound speed, which is sufficient to keep the clouds in approximate virial equilibrium for many free-fall times. The virial parameter, α_V, defined as twice the clump kinetic energy, $2E$, divided by the clump gravitational potential energy, U, is larger than 1 for L1551, implying that outflows can disrupt this clump. However, $\dot{P}_{\rm out}/\dot{P}_{\rm turb}$ declines with increasing mass and the virial parameter for most clumps is less than 1. Nakamura & Li (2014) define a parameter, $\eta_{\rm out} = 2E_{\rm out}/U$, where $E_{\rm out}$ is the total outflow kinetic energy, finding that, except for L1551, $\eta_{\rm out} < 1$, implying that although outflows can maintain virial equilibrium, they can't disrupt most clumps. However, this analysis only takes into account the molecular component of outflows.

Several factors make outflow feedback potentially more important. Outflow masses and momenta may be underestimated when based only on low-*J* CO (Dunham et al. 2014). ISO and *Herschel* have shown the presence of warm and hot molecular gas (van Kempen et al. 2010). Mid-IR studies show that high-*J* CO originates in hot, >2,000 K, subthermally excited $n(H_2) < 10^6$ cm^{-3} gas (Goicoechea et al. 2012, Herczeg et al. 2012, Manoj et al. 2013). Shocked H_2 also implies gas with temperatures of 2,000–3,000 K. Depending on the magnetic field strength, molecules tend to be destroyed at shock speeds ~10 to 100 km s^{-1}; mass and velocity measurements based on molecules miss the faster atomic and ionized components. Although CO and other molecules are effective in the determination of momentum injection rates in Class 0 and early Class I phases, these tracers are less effective in evolved systems as their outflows blow out of their parent cores. The decline in momentum injection rates from Class 0 to I may in part reflect this observational selection effect. Declining accretion and consequent mass-loss rates can be partially offset by increasing ejection velocity as stellar radii and outflow launch points shrink as the YSOs approach the main sequence. Some YSOs may produce wide-angle winds whose densities decline faster than collimated flows, making direct detection difficult. Expanding parsec-scale cavities in GMCs may be produced by such winds (Arce et al. 2011, Nakamura et al. 2012). Most stars form in multiple-star systems and clusters in which stellar motion in the potential well and N-body interactions can alter outflow orientations as evidenced by S-shaped point-symmetric flows. Variations in degree of collimation and flow orientation, isotropic wide-angle flows, and explosions similar to Orion can inject momentum into clouds over a large solid angle. Finally, hot, mega-Kelvin, X-ray plasmas in outflow cocoons formed behind shocks with speeds greater than 400 km s^{-1} have long cooling times, and their adiabatic expansion can conserve energy.

Far ultraviolet (FUV): 912 Å < $\lambda \lesssim$ 3,000 Å that does not ionize hydrogen

If outflow feedback fails to stop star formation and the clump continues to contract, star formation can continue. As stellar mass grows past a few Solar masses, their pre-main-sequence lifetimes shrink to less than 10^6 years (Zinnecker & Yorke 2007), and far-UV (FUV) radiation from moderate-mass stars can provide additional feedback. These stars emit FUV radiation that heats cloud surfaces to ~10^3 K, and the resulting pressure gradients can accelerate gas to a few km s^{-1}.

Where the sound-speed is larger than the escape speed, the gas can become unbound. If FUV fails to disrupt the cloud, massive stars with $M_* > 8\ M_\odot$, whose extreme-UV (EUV) radiation ionizes hydrogen, raises the sound speed to ~10 km s^{-1}. Clouds with lower escape speeds will lose the plasma. In most Galactic star-forming regions, the emergence of OB stars stops star formation. However, in extremely dense and massive clouds with escape speeds greater than ~10 to 20 km s^{-1}, OB-star winds, radiation pressure, or supernovae may be needed to halt star formation. In these extreme cases, the star-formation efficiency is likely to be greater than 30%, leading to the formation of bound clusters. Failure of feedback in massive, compact GMCs may be the recipe for the formation of tightly bound clusters such as globular clusters.

Extreme ultraviolet (EUV): $\lambda < 912$ Å (13.6 eV) that does ionize hydrogen

5. SUMMARY & FUTURE PROSPECTS

Protostellar outflows are multiphase, dynamic, evolving systems that provide fossil records of the accretion histories of the source stars. A complete characterization of the protostellar outflows requires molecular, atomic, and ionic tracers throughout the spectrum sensitive to a wide range in temperatures, densities, and column densities. Outflow structure indicates that accretion is episodic with interludes of quiescence. Low levels of outflow activity, and by inference accretion, persist for millions of years. Outflow-orientation changes indicate that many stars form in dynamically complex environments where sibling stars drive forced precession and accretion flow directions vary over time. Although most outflows are collimated and bipolar, some, especially massive ones such as those in OMC1, experience short-lived explosive behavior.

The youngest YSOs eject molecule-dominated jets that sweep up surrounding gas into shells. As YSOs evolve and outflows age, molecular lobes tend to be confined to the parent core or clump while atomic and ionic constituents grow to parsec-scale dimensions. Subarcsecond ALMA, adaptive optics–assisted, space-based near-IR, and visual observations enable proper motion measurements of jets, bullets, and other compact structures over time intervals of only a few years in nearby sources. Combined with radial velocities, proper motions provide 3D velocity vectors. Deep X-ray, visual, and IR imaging and spectroscopy of ionic and atomic species are required to trace the fastest and hottest components in outflows. The *James Webb Space Telescope* (JWST) will have the sensitivity to detect the low-emission components of outflows in tracers, such as the 4.05-μm Brackett-α line, and to detect absorption from low-density atomic and ionized components against background sources using spectroscopy of the mid-IR pure rotational transitions of H_2 as well as providing unprecedented sensitivity for [FeII] and rovibrational H_2 studies. JWST and ALMA will investigate outflows in the Galaxy's central molecular zone and in star-forming regions in nearby galaxies. As analysis methods, understanding of abundances, and optical depths improve, and as observations of the atomic and ionized components become more sensitive, the momentum injection rates and impacts of outflows will become better constrained. Advanced MHD and HD codes with larger dynamic ranges in parameters are needed to model the full range of outflow phenomena from stellar-scales to parsec-scales, clustering, and interactions in multiples and clusters.

FUTURE ISSUES

1. Large-scale, systematic surveys of outflows are still needed in multiple tracers using identical data acquisition, reduction, and analysis methods to measure masses, momentum injection rates, and other physical properties of outflows as functions of environment, YSO age, mass, and evolutionary stage.

2. More mid-IR surveys of the high-J transitions of CO, H_2O, and OH as well as mid-IR surveys of fine-structure cooling lines such as 63 μm[OI] with platforms such as SOFIA, balloons, or satellites are needed.
3. Narrow-band surveys in the near-IR of H_2, [FeII], and hydrogen recombination lines from space with facilities such as JWST will provide unprecedented sensitivity and resolution for tracing the full extents of flows. Absorption line studies against suitable background sources are needed to identify low-density outflow components.
4. Sensitive, narrow-band surveys of HH objects must be continued to identify shocks and measure proper motions.
5. Multiobject and integral-field spectroscopic surveys are needed of HH objects and their source stars to measure radial velocities, densities, and excitation conditions as well as to identify variations.
6. Synoptic monitoring for flares from YSOs and MYSOs in the Galaxy and nearby galaxies are needed to establish a clear link between accretion and outflow and to search for luminous IR flares from Orion-like events.
7. The transition from protostellar to main-sequence outflows requires investigation, especially for moderate-mass and massive stars.

DISCLOSURE STATEMENT

The author is not aware of any affiliations, memberships, funding, or financial holdings that might be perceived as affecting the objectivity of this review.

ACKNOWLEDGMENTS

The author thanks Michael Dunham, Adam Ginsburg, Wayne Green, Doug Johnstone, Lars Kristensen, Charlie Lada, Luke Maud, Bo Reipurth, Ewine van Dishoeck, and Hans Zinnecker for excellent comments and for discussions that greatly improved this manuscript. J.B. thanks Kim Ruhland and Christine Green for careful proofreading and editing. This work was supported in part by National Science Foundation (NSF) grant AST-1009847. This paper uses ALMA data obtained with program ADS/JAO.ALMA #2013.1.00546.S. ALMA is a partnership of the European Southern Observatory (ESO) representing member states, Associated Universities, Inc. (AUI), and the National Radio Astronomy Observatories (NRAO) for the NSF in the United States, the National Institutes of Natural Sciences in Japan, the National Research Council in Canada, and the National Science Council and the Academia Sinica Institute of Astronomy and Astrophysics in Taiwan, in cooperation with the Republic of Chile. The Joint ALMA Observatory (JAO) is operated by the ESO (Europe), the AUI/NRAO (USA), and the National Astronomical Observatory of Japan (Japan).

LITERATURE CITED

Allen DA, Burton MG. 1993. *Nature* 363:54–56
Anderl S, Guillet V, Pineau des Forêts G, Flower DR. 2013. *Astron. Astrophys.* 556:A69
Andrews SM, Reipurth B, Bally J, Heathcote SR. 2004. *Ap. J.* 606:353–68
Arce HG, Borkin MA, Goodman AA, Pineda JE, Beaumont CN. 2011. *Ap. J.* 742:105

Arce HG, Borkin MA, Goodman AA, Pineda JE, Halle MW. 2010. *Ap. J.* 715:1170–90
Arce HG, Mardones D, Corder SA, et al. 2013. *Ap. J.* 774:39
Armond T, Reipurth B, Bally J, Aspin C. 2011. *Astron. Astrophys.* 528:A125
Bachiller R. 1996. *Annu. Rev. Astron. Astrophys.* 34:111–54
Bachiller R, Fuente A, Tafalla M. 1995. *Ap. J. Lett.* 445:L51–54
Ball JA, Gottlieb CA, Lilley AE, Radford HE. 1970. *Ap. J. Lett.* 162:L203
Bally J, Cunningham NJ, Moeckel N, et al. 2011. *Ap. J.* 727:113
Bally J, Devine D. 1994. *Ap. J. Lett.* 428:L65–68
Bally J, Devine D, Alten V, Sutherland RS. 1997. *Ap. J.* 478:603–13
Bally J, Devine D, Reipurth B. 1996. *Ap. J. Lett.* 473:L49–53
Bally J, Ginsburg A, Probst R, et al. 2014. *Astron. J.* 148:120
Bally J, Ginsburg A, Silvia D, Youngblood A. 2015. *Astron. Astrophys.* 579:A130
Bally J, Lada CJ. 1983. *Ap. J.* 265:824–47
Bally J, Langer WD, Stark AA, Wilson RW. 1987. *Ap. J. Lett.* 312:L45
Bally J, Licht D, Smith N, Walawender J. 2006a. *Astron. J.* 131:473–500
Bally J, Reipurth B. 2001. *Ap. J.* 546:299–323
Bally J, Stark AA. 1983. *Ap. J. Lett.* 266:L61–64
Bally J, Walawender J, Luhman KL, Fazio G. 2006b. *Astron. J.* 132:1923–37
Bally J, Walawender J, Reipurth B. 2012a. *Astron. J.* 144:143
Bally J, Youngblood A, Ginsburg A. 2012b. *Ap. J.* 756:137
Bally J, Zinnecker H. 2005. *Astron. J.* 129:2281–93
Becklin EE, Neugebauer G. 1967. *Ap. J.* 147:799
Beuther H, Nissen HD. 2008. *Ap. J. Lett.* 679:L121–24
Bieging JH, Revelle M, Peters WL. 2014. *Ap. J. Suppl.* 214:7
Bjerkeli P, Liseau R, Larsson B, et al. 2012. *Astron. Astrophys.* 546:A29
Bontemps S, Andre P, Terebey S, Cabrit S. 1996. *Astron. Astrophys.* 311:858–72
Bourke TL. 2001. *Ap. J. Lett.* 554:L91–94
Busquet G, Lefloch B, Benedettini M, et al. 2014. *Astron. Astrophys.* 561:A120
Cabrit S. 2007. In *MHD jets and winds from young stars*, *Lect. Notes Phys.* Vol. 723, ed. J Ferreira, C Dougados, E Whelan, p. 21. Berlin: Springer-Verlag
Cabrit S, Raga A. 2000. *Astron. Astrophys.* 354:667–73
Cantó J, Rodriguéz LF. 1980. *Ap. J.* 239:982–87
Cantó J, Rodriguéz LF, Barral JF, Carral P. 1981. *Ap. J.* 244:102–14
Caratti o Garatti A, Stecklum B, Linz H, Garcia Lopez R, Sanna A. 2015. *Astron. Astrophys.* 573:A82
Carroll JJ, Frank A, Blackman EG, Cunningham AJ, Quillen AC. 2009. *Ap. J.* 695:1376–81
Cernicharo J, Lefloch B, Cox P, et al. 1998. *Science* 282:462
Chatterjee S, Tan JC. 2012. *Ap. J.* 754:152
Chen X, Gan CG, Ellingsen SP, et al. 2013a. *Ap. J. Suppl.* 206:9
Chen X, Gan CG, Ellingsen SP, et al. 2013b. *Ap. J. Suppl.* 206:22
Chernin LM, Masson CR. 1995. *Ap. J.* 443:181–86
Cheung AC, Rank DM, Townes CH, Thornton DD, Welch WJ. 1969. *Nature* 221:626–28
Codella C, Cabrit S, Gueth F, et al. 2007. *Astron. Astrophys.* 462:L53–56
Codella C, Cabrit S, Gueth F, et al. 2014. *Astron. Astrophys.* 568:L5
Cohen M, Bieging JH, Schwartz PR. 1982. *Ap. J.* 253:707–15
Colgan SWJ, Schultz ASB, Kaufman MJ, Erickson EF, Hollenbach DJ. 2007. *Ap. J.* 671:536–45
Colín P, Vázquez-Semadeni E, Gómez GC. 2013. *MNRAS* 435:1701–14
Corradi RLM, Grosso N, Acker A, Greimel R, Guillout P. 2014. *Astron. Astrophys.* 570:A105
Cunningham NJ, Moeckel N, Bally J. 2009. *Ap. J.* 692:943–54
Curiel S, Ho PTP, Patel NA, et al. 2006. *Ap. J.* 638:878–86
Curtis EI, Richer JS, Swift JJ, Williams JP. 2010. *MNRAS* 408:1516–39
Cyganowski CJ, Whitney BA, Holden E, et al. 2008. *Astron. J.* 136:2391–412
Davis CJ, Froebrich D, Stanke T, et al. 2009. *Astron. Astrophys.* 496:153–76
Davis CJ, Gell R, Khanzadyan T, Smith MD, Jenness T. 2010. *Astron. Astrophys.* 511:A24

De Buizer JM, Morris MR, Becklin EE, et al. 2012. *Ap. J. Lett.* 749:L23
De Colle F, Raga AC. 2005. *MNRAS* 359:164–70
Devine D, Bally J, Reipurth B, Heathcote S. 1997. *Astron. J.* 114:2095
Devine D, Grady CA, Kimble RA, et al. 2000. *Ap. J. Lett.* 542:L115–18
Dopita MA, Evans I, Schwartz RD. 1982. *Ap. J. Lett.* 263:L73–77
Downes TP, Downes S. 2007. *Astron. Astrophys.* 471:873–84
Drabek-Maunder E, Hatchell J, Buckle JV, Di Francesco J, Richer J. 2016. *MNRAS* 457:L84–88
Draine BT. 2011. *Physics of the Interstellar and Intergalactic Medium*. Princeton, NJ: Princeton Univ. Press
Draine BT, McKee CF. 1993. *Annu. Rev. Astron. Astrophys.* 31:373–432
Duarte-Cabral A, Bontemps S, Motte F, et al. 2013. *Astron. Astrophys.* 558:A125
Duarte-Cabral A, Chrysostomou A, Peretto N, et al. 2012. *Astron. Astrophys.* 543:A140
Dunham MM, Arce HG, Mardones D, et al. 2014. *Ap. J.* 783:29
Dunham MM, Chen X, Arce HG, et al. 2011. *Ap. J.* 742:1
Eislöffel J. 2000. *Astron. Astrophys.* 354:236–46
Eislöffel J, Mundt R. 1997. *Astron. J.* 114:280–87
Eislöffel J, Nisini B, Güsten R, Wiesemeyer H, Gusdorf A. 2012. *Astron. Astrophys.* 542:L11
Ellerbroek LE, Podio L, Kaper L, et al. 2013. *Astron. Astrophys.* 551:A5
Elmegreen BG. 2007. *Ap. J.* 668:1064–82
Elmegreen BG, Scalo J. 2004. *Annu. Rev. Astron. Astrophys.* 42:211–73
Erickson NR, Goldsmith PF, Snell RL, et al. 1982. *Ap. J. Lett.* 261:L103–7
Evans NJ II, Dunham MM, Jørgensen JK, et al. 2009. *Ap. J. Suppl.* 181:321–50
Federrath C, Schrön M, Banerjee R, Klessen RS. 2014. *Ap. J.* 790:128
Fernández-López M, Girart JM, Curiel S, et al. 2013. *Ap. J.* 778:72
Flower DR, Pineau des Forêts G. 2010. *MNRAS* 406:1745–58
Flower DR, Pineau des Forêts G. 2015. *Astron. Astrophys.* 578:A63
Frank A, Ray TP, Cabrit S, et al. 2014. In *Protostars and Planets VI*, ed. H Beuther, RS Klessen, CP Dullemond, T Henning, pp. 451–74. Tucson: Univ. Ariz. Press
Froebrich D, Makin SV, Davis CJ, et al. 2015. *MNRAS* 454:2586–605
Froebrich D, Smith MD, Eislöffel J. 2002. *Astron. Astrophys.* 385:239–56
Fukui Y, Iwata T, Mizuno A, Bally J, Lane AP. 1993. In *Protostars and Planets III*, ed. EH Levy, JI Lunine, pp. 603–39. Tucson: Univ. Ariz. Press
Furuya RS, Shinnaga H. 2009. *Ap. J.* 703:1198–202
Gålfalk M, Olofsson G, Kaas AA, et al. 2004. *Astron. Astrophys.* 420:945–55
Garay G, Brooks KJ, Mardones D, Norris RP. 2003. *Ap. J.* 587:739–47
Garay G, Mardones D, Bronfman L, et al. 2007. *Astron. Astrophys.* 463:217–24
Garcia Lopez R, Nisini B, Eislöffel J, et al. 2010. *Astron. Astrophys.* 511:A5
Genzel R, Stutzki J. 1989. *Annu. Rev. Astron. Astrophys.* 27:41–85
Gerin M, Neufeld DA, Goicoechea JR. 2016. *Annu. Rev. Astron. Astrophys.* 54:181–225
Gerin M, Pety J, Fuente A, et al. 2015. *Astron. Astrophys.* 577:L2
Giannini T, Nisini B, Neufeld D, et al. 2011. *Ap. J.* 738:80
Ginsburg A, Bally J, Battersby C, et al. 2015. *Astron. Astrophys.* 573:A106
Ginsburg AG, Bally J, Yan CH, Williams JP. 2009. *Ap. J.* 707:310–27
Goddi C, Humphreys EML, Greenhill LJ, Chandler CJ, Matthews LD. 2011. *Ap. J.* 728:15
Goicoechea JR, Cernicharo J, Karska A, et al. 2012. *Astron. Astrophys.* 548:A77
Goicoechea JR, Chavarría L, Cernicharo J, et al. 2015. *Ap. J.* 799:102
Gómez L, Rodríguez LF, Loinard L, et al. 2005. *Ap. J.* 635:1166–72
Gómez L, Rodríguez LF, Loinard L, et al. 2008. *Ap. J.* 685:333–43
Gómez-Ruiz AI, Gusdorf A, Leurini S, et al. 2012. *Astron. Astrophys.* 542:L9
Grady CA, Devine D, Woodgate B, et al. 2000. *Ap. J.* 544:895–902
Greenhill LJ, Gwinn CR, Schwartz C, Moran JM, Diamond PJ. 1998. *Nature* 396:650–53
Grosso N, Feigelson ED, Getman KV, et al. 2006. *Astron. Astrophys.* 448:L29–32
Günther HM, Li ZY, Schneider PC. 2014. *Ap. J.* 795:51
Gusdorf A, Guesten R, Menten KM, et al. 2016. *Astron. Astrophys.* 585:A45

Guszejnov D, Krumholz MR, Hopkins PF. 2016. *MNRAS* 458:673–80
Haro G. 1952. *Ap. J.* 115:572
Hartigan P, Edwards S, Ghandour L. 1995. *Ap. J.* 452:736
Hartigan P, Frank A, Foster JM, et al. 2011. *Ap. J.* 736:29
Hartmann L, Burkert A. 2007. *Ap. J.* 654:988–97
Hatchell J, Dunham MM. 2009. *Astron. Astrophys.* 502:139–53
Hatchell J, Wilson T, Drabek E, et al. 2013. *MNRAS* 429:L10–14
Heathcote S, Morse JA, Hartigan P, et al. 1996. *Astron. J.* 112:1141
Henney WJ, O'Dell CR, Zapata LA, et al. 2007. *Astron. J.* 133:2192–205
Henning T, Lapinov A, Schreyer K, Stecklum B, Zinchenko I. 2000. *Astron. Astrophys.* 364:613–24
Herbig GH. 1951. *Ap. J.* 113:697–99
Herbig GH. 1960. *Ap. J. Suppl.* 4:337
Herczeg GJ, Karska A, Bruderer S, et al. 2012. *Astron. Astrophys.* 540:A84
Higuchi AE, Saigo K, Chibueze JO, et al. 2015. *Ap. J. Lett.* 798:L33
Hollenbach D, McKee CF. 1989. *Ap. J.* 342:306–36
Hosokawa T, Omukai K. 2009. *Ap. J.* 691:823–46
Hosokawa T, Yorke HW, Omukai K. 2010. *Ap. J.* 721:478–92
Ioannidis G, Froebrich D. 2012a. *MNRAS* 421:3257–65
Ioannidis G, Froebrich D. 2012b. *MNRAS* 425:1380–93
Jaffe DT, Martín-Pintado J. 1999. *Ap. J.* 520:162–72
Jiménez-Serra I, Martín-Pintado J, Báez-Rubio A, Patel N, Thum C. 2011. *Ap. J. Lett.* 732:L27
Joy AH. 1945. *Ap. J.* 102:168
Karska A, Herczeg GJ, van Dishoeck EF, et al. 2013. *Astron. Astrophys.* 552:A141
Karska A, Herpin F, Bruderer S, et al. 2014a. *Astron. Astrophys.* 562:A45
Karska A, Kristensen LE, van Dishoeck EF, et al. 2014b. *Astron. Astrophys.* 572:A9
Keto E. 2003. *Ap. J.* 599:1196–206
Klaassen PD, Wilson CD. 2007. *Ap. J.* 663:1092–102
Klaassen PD, Wilson CD. 2008. *Ap. J.* 684:1273–80
Kleinmann DE, Low FJ. 1967. *Ap. J. Lett.* 149:L1
Königl A. 1991. *Ap. J. Lett.* 370:L39–43
Königl A, Romanova MM, Lovelace RVE. 2011. *MNRAS* 416:757–66
Königl A, Salmeron R, Salmeron M. 2010. *MNRAS* 401:479–99
Kristensen LE, van Dishoeck EF, Bergin EA, et al. 2012. *Astron. Astrophys.* 542:A8
Kristensen LE, van Dishoeck EF, Tafalla M, et al. 2011. *Astron. Astrophys.* 531:L1
Kristensen LE, Visser R, van Dishoeck EF, et al. 2010. *Astron. Astrophys.* 521:L30
Krumholz MR, Klein RI, McKee CF. 2011. *Ap. J.* 740:74
Kwan J, Scoville N. 1976. *Ap. J. Lett.* 210:L39–43
Lacy JH, Jaffe DT, Zhu Q, et al. 2007. *Ap. J. Lett.* 658:L45–49
Lada CJ. 1985. *Annu. Rev. Astron. Astrophys.* 23:267–317
Lada CJ, Alves J, Lada EA. 1996. *Astron. J.* 111:1964
Lada CJ, Lada EA. 2003. *Annu. Rev. Astron. Astrophys.* 41:57–115
Lee CF, Hirano N, Palau A, et al. 2009. *Ap. J.* 699:1584–94
Lee CF, Ho PTP, Beuther H, et al. 2006. *Ap. J.* 639:292–302
Lee CF, Ho PTP, Bourke TL, et al. 2008. *Ap. J.* 685:1026–32
Lee CF, Ho PTP, Hirano N, et al. 2007. *Ap. J.* 659:499–511
Lee CF, Mundy LG, Reipurth B, Ostriker EC, Stone JM. 2000. *Ap. J.* 542:925–45
Lee CF, Rao R, Ching TC, et al. 2014. *Ap. J. Lett.* 797:L9
Lee HT, Liao WT, Froebrich, et al. 2013. *Ap. J. Suppl. Ser.* 208:23
Lee HT, Takami M, Duan HY, et al. 2012. *Ap. J. Suppl. Ser.* 200:2
Lee JK, Burton MG. 2000. *MNRAS* 315:11–20
Lerate MR, Barlow MJ, Swinyard BM, et al. 2006. *MNRAS* 370:597–628
Lerate MR, Yates J, Viti S, et al. 2008. *MNRAS* 387:1660–68

Li ZY, Banerjee R, Pudritz RE, et al. 2014. In *Protostars and Planets VI*, ed. H Beuther, RS Klessen, CP Dullemond, T Henning, pp. 173–94. Tucson: Univ. Ariz. Press
Livio M. 2011. In *Gamma Ray Bursts 2010*, ed. JE McEnery, JL Racusin, N Gehrels. *AIP Conf. Ser.* 1358:329. Melville, NY: AIP
Lumsden SL, Wheelwright HE, Hoare MG, Oudmaijer RD, Drew JE. 2012. *MNRAS* 424:1088–104
Manoj P, Watson DM, Neufeld DA, et al. 2013. *Ap. J.* 763:83
Maret S, Bergin EA, Neufeld DA, et al. 2009. *Ap. J.* 698:1244–60
Martí J, Rodríguez LF, Reipurth B. 1998. *Ap. J.* 502:337–41
Masciadri E, de Gouveia Dal Pino EM, Raga AC, Noriega-Crespo A. 2002. *Ap. J.* 580:950–58
Masqué JM, Girart JM, Estalella R, Rodríguez LF, Beltrán MT. 2012. *Ap. J. Lett.* 758:L10
Masqué JM, Rodríguez LF, Araudo A, et al. 2015. *Ap. J.* 814:44
Matzner CD. 2007. *Ap. J.* 659:1394–403
Matzner CD, Jumper PH. 2015. *Ap. J.* 815:68
Matzner CD, McKee CF. 1999. *Ap. J. Lett.* 526:L109–12
Maud LT, Lumsden SL, Moore TJT. 2015a. *MNRAS* 452:637–55
Maud LT, Moore TJT, Lumsden SL, et al. 2015b. *MNRAS* 453:645–65
McKee CF, Draine BT. 1991. *Science* 252:397–403
McKee CF, Hollenbach DJ. 1980. *Annu. Rev. Astron. Astrophys.* 18:219–62
Menten KM, Reid MJ. 1995. *Ap. J. Lett.* 445:L157–60
Menten KM, Reid MJ, Forbrich J, Brunthaler A. 2007. *Astron. Astrophys.* 474:515–20
Merello M, Bronfman L, Garay G, et al. 2013. *Ap. J. Lett.* 774:L7
Mohanty S, Shu FH. 2008. *Ap. J.* 687:1323–38
Molinari S, Noriega-Crespo A. 2002. *Astron. J.* 123:2010–18
Molinari S, Noriega-Crespo A, Ceccarelli C, et al. 2000. *Ap. J.* 538:698–709
Morino JI, Yamashita T, Hasegawa T, Nakano T. 1998. *Nature* 393:340–42
Morris PW, Noriega-Crespo A, Marleau FR, et al. 2004. *Ap. J. Suppl.* 154:339–45
Mottram JC, Kristensen LE, van Dishoeck EF, et al. 2014. *Astron. Astrophys.* 572:A21
Mundt R. 1984. *Ap. J.* 280:749–70
Mundt R, Fried JW. 1983. *Ap. J. Lett.* 274:L83–86
Myers AT, Klein RI, Krumholz MR, McKee CF. 2014. *MNRAS* 439:3420–38
Nakamura F, Kamada Y, Kamazaki T, et al. 2011. *Ap. J.* 726:46
Nakamura F, Li ZY. 2007. *Ap. J.* 662:395–412
Nakamura F, Li ZY. 2011. *Ap. J.* 740:36
Nakamura F, Li ZY. 2014. *Ap. J.* 783:115
Nakamura F, Miura T, Kitamura Y, et al. 2012. *Ap. J.* 746:25
Natta A, Testi L, Alcalá JM, et al. 2014. *Astron. Astrophys.* 569:A5
Neufeld DA, Nisini B, Giannini T, et al. 2009. *Ap. J.* 706:170–83
Nisini B, Benedettini M, Codella C, et al. 2010a. *Astron. Astrophys.* 518:L120
Nisini B, Codella C, Giannini T, et al. 2007. *Astron. Astrophys.* 462:163–72
Nisini B, Giannini T, Neufeld DA, et al. 2010b. *Ap. J.* 724:69–79
Nisini B, Santangelo G, Antoniucci S, et al. 2013. *Astron. Astrophys.* 549:A16
Nisini B, Santangelo G, Giannini T, et al. 2015. *Ap. J.* 801:121
Nissen HD, Gustafsson M, Lemaire JL, et al. 2007. *Astron. Astrophys.* 466:949–68
Noriega-Crespo A, Morris P, Marleau FR, et al. 2004. *Ap. J. Suppl.* 154:352–58
O'Dell CR. 2001. *Annu. Rev. Astron. Astrophys.* 39:99–136
O'Dell CR, Ferland GJ, Henney WJ, et al. 2015. *Astron. J.* 150:108
Offner SSR, Lee EJ, Goodman AA, Arce H. 2011. *Ap. J.* 743:91
Ogura K. 1991. *Astron. J.* 101:1803–6
Ogura K. 1995. *Ap. J. Lett.* 450:L23–26
Padoan P, Juvela M, Kritsuk A, Norman ML. 2009. *Ap. J. Lett.* 707:L153–57
Pascucci I, Edwards S, Heyer M, et al. 2015. *Ap. J.* 814:14
Peng TC, Wyrowski F, Zapata LA, Güsten R, Menten KM. 2012. *Astron. Astrophys.* 538:A12
Phan-Bao N, Lee CF, Ho PTP, Dang-Duc C, Li D. 2014a. *Ap. J.* 795:70

Phan-Bao N, Lee CF, Ho PTP, Martín EL. 2014b. *Astron. Astrophys.* 564:A32
Plambeck RL, Wright MCH, Friedel DN, et al. 2009. *Ap. J. Lett.* 704:L25–28
Plambeck RL, Wright MCH, Mundy LG, Looney LW. 1995. *Ap. J. Lett.* 455:L189–92
Plunkett AL, Arce HG, Corder SA, et al. 2013. *Ap. J.* 774:22
Plunkett AL, Arce HG, Corder SA, et al. 2015. *Ap. J.* 803:22
Podio L, Codella C, Gueth F, et al. 2015. *Astron. Astrophys.* 581:A85
Pravdo SH, Feigelson ED, Garmire G, et al. 2001. *Nature* 413:708–11
Pravdo SH, Tsuboi Y. 2005. *Ap. J.* 626:272–82
Pravdo SH, Tsuboi Y, Maeda Y. 2004. *Ap. J.* 605:259–71
Pravdo SH, Tsuboi Y, Uzawa A, Ezoe Y. 2009. *Ap. J.* 704:1495–505
Price DJ, Tricco TS, Bate MR. 2012. *MNRAS* 423:L45–49
Pudritz RE, Ouyed R, Fendt C, Brandenburg A. 2007. See Reipurth et al. 2007, pp. 277–94
Qiu K, Zhang Q. 2009. *Ap. J. Lett.* 702:L66–71
Quillen AC, Thorndike SL, Cunningham A, et al. 2005. *Ap. J.* 632:941–55
Raga A, Noriega-Crespo A. 1998. *Astron. J.* 116:2943–52
Raga AC, Binette L, Canto J, Calvet N. 1990. *Ap. J.* 364:601–10
Raga AC, Noriega-Crespo A, Kajdic P, et al. 2011a. *Rev. Mex. Astron. Astrofis.* 47:277–88
Raga AC, Noriega-Crespo A, Rodríguez-González A, et al. 2012a. *Ap. J.* 748:103
Raga AC, Reipurth B, Cantó J, Sierra-Flores MM, Guzmán MV. 2011b. *Rev. Mex. Astron. Astrofis.* 47:425–37
Raga AC, Reipurth B, Castellanos-Ramírez A, Chiang HF, Bally J. 2015. *Ap. J. Lett.* 798:L1
Raga AC, Rodríguez-González A, Noriega-Crespo A, Esquivel A. 2012b. *Ap. J. Lett.* 744:L12
Raga AC, Velázquez PF, Cantó J, Masciadri E. 2002. *Astron. Astrophys.* 395:647–56
Ray T, Dougados C, Bacciotti F, Eislöffel J, Chrysostomou A. 2007. See Reipurth et al. 2007, pp. 231–44
Reipurth B. 2000. *Astron. J.* 120:3177–91
Reipurth B. 2016. *George Herbig and Early Stellar Evolution. Inst. Astron. Spec. Publ., No. 1*, Univ. Hawaii, Hilo, HI
Reipurth B, Aspin C, Bally J, Tobin JJ, Walawender J. 2010. *Astron. J.* 140:699–712
Reipurth B, Bally J. 2001. *Annu. Rev. Astron. Astrophys.* 39:403–55
Reipurth B, Bally J, Aspin C, et al. 2013. *Astron. J.* 146:118
Reipurth B, Bally J, Devine D. 1997a. *Astron. J.* 114:2708
Reipurth B, Bally J, Fesen RA, Devine D. 1998a. *Nature* 396:343–45
Reipurth B, Bally J, Graham JA, Lane AP, Zealey WJ. 1986. *Astron. Astrophys.* 164:51–66
Reipurth B, Devine D, Bally J. 1998b. *Astron. J.* 116:1396–411
Reipurth B, Hartigan P, Heathcote S, Morse JA, Bally J. 1997b. *Astron. J.* 114:757–80
Reipurth B, Heathcote S, Morse J, Hartigan P, Bally J. 2002. *Astron. J.* 123:362–81
Reipurth B, Jewitt D, Keil K, eds. 2007. *Protostars and Planets V*. Tucson: Univ. Ariz. Press
Reipurth B, Mikkola S. 2012. *Nature* 492:221–24
Riaz B, Thompson M, Whelan ET, Lodieu N. 2015. *MNRAS* 446:2550–59
Rodriguéz LF, Escalante V, Lizano S, Canto J, Mirabel IF. 1990. *Ap. J.* 365:261–68
Rodríguez LF, Garay G, Brooks KJ, Mardones D. 2005. *Ap. J.* 626:953–58
Rodríguez LF, Moran JM, Franco-Hernández R, et al. 2008. *Astron. J.* 135:2370–79
Rodríguez LF, Zapata LA, Ho PTP. 2009. *Ap. J.* 692:162–67
Rodríguez-Kamenetzky A, Carrasco-González C, Araudo A, et al. 2015. *Ap. J.* 818:27
Rosenthal D, Bertoldi F, Drapatz S. 2000. *Astron. Astrophys.* 356:705–23
Russell APG, Bally J, Padman R, Hills RE. 1992. *Ap. J.* 387:219–28
Rydgren AE, Strom SE, Strom KM. 1976. *Ap. J. Suppl.* 30:307–36
Sahai R, Claussen M, Sánchez Contreras C, Morris M, Sarkar G. 2008. *Ap. J.* 680:483–94
San José-García I, Mottram JC, Kristensen LE, et al. 2013. *Astron. Astrophys.* 553:A125
San Jose-Garcia I, Mottram JC, van Dishoeck EF, et al. 2015. *Astron. Astrophys.* 585:A103
Sánchez-Monge Á, Beltrán MT, Cesaroni R, et al. 2014. *Astron. Astrophys.* 569:A11
Santangelo G, Nisini B, Antoniucci S, et al. 2013. *Astron. Astrophys.* 557:A22
Santangelo G, Nisini B, Codella C, et al. 2014. *Astron. Astrophys.* 568:A125
Scalo J, Elmegreen BG. 2004. *Annu. Rev. Astron. Astrophys.* 42:275–316

Schneider PC, Günther HM, Schmitt JHMM. 2009. *Astron. Astrophys.* 508:717–24
Schneider PC, Günther HM, Schmitt JHMM. 2011. *Astron. Astrophys.* 530:A123
Scoville N, Kleinmann SG, Hall DNB, Ridgway ST. 1983. *Ap. J.* 275:201–24
Shang H, Li ZY, Hirano N. 2007. See Reipurth et al. 2007, pp. 261–76
Shu FH, Lizano S, Ruden SP, Najita J. 1988. *Ap. J. Lett.* 328:L19–23
Shu FH, Najita JR, Shang H, Li ZY. 2000. In *Protostars and Planets IV*, ed. V Mannings, AP Boss, SS Russell, pp. 789–814. Tucson: Univ. Ariz. Press
Shu FH, Ruden SP, Lada CJ, Lizano S. 1991. *Ap. J. Lett.* 370:L31–34
Simon M, Felli M, Cassar L, Fischer J, Massi M. 1983. *Ap. J.* 266:623–45
Smith MD, Eislöffel J, Davis CJ. 1998. *MNRAS* 297:687–91
Smith N, Bally J, Walborn NR. 2010. *MNRAS* 405:1153–86
Smith N, Whitney BA, Conti PS, de Pree CG, Jackson JM. 2009. *MNRAS* 399:952–65
Snell RL, Bally J. 1986. *Ap. J.* 303:683–701
Snell RL, Loren RB, Plambeck RL. 1980. *Ap. J. Lett.* 239:L17–22
Snell RL, Scoville NZ, Sanders DB, Erickson NR. 1984. *Ap. J.* 284:176–93
Stanke T, McCaughrean MJ, Zinnecker H. 1999. *Astron. Astrophys.* 350:L43–46
Stojimirović I, Narayanan G, Snell RL, Bally J. 2006. *Ap. J.* 649:280–98
Stojimirović I, Snell RL, Narayanan G. 2008. *Ap. J.* 679:557–69
Tafalla M, Liseau R, Nisini B, et al. 2013. *Astron. Astrophys.* 551:A116
Takahashi S, Ohashi N, Bourke TL. 2013. *Ap. J.* 774:20
Takahashi S, Saito M, Ohashi N, et al. 2008. *Ap. J.* 688:344–61
Tan JC, Krumholz MR, McKee CF. 2006. *Ap. J. Lett.* 641:L121–24
Tappe A, Forbrich J, Martín S, Yuan Y, Lada CJ. 2012. *Ap. J.* 751:9
Testi L, Tan JC, Palla F. 2010. *Astron. Astrophys.* 522:A44
Tobin JJ, Dunham MM, Looney LW, et al. 2015. *Ap. J.* 798:61
Torrelles JM, Patel NA, Curiel S, et al. 2011. *MNRAS* 410:627–40
Tsitali AE, Belloche A, Commerçon B, Menten KM. 2013. *Astron. Astrophys.* 557:A98
van den Ancker ME, Wesselius PR, Tielens AGGM, van Dishoeck EF, Spinoglio L. 1999. *Astron. Astrophys.* 348:877–87
van der Marel N, Kristensen LE, Visser R, et al. 2013. *Astron. Astrophys.* 556:A76
van Dishoeck EF, Herbst E, Neufeld DA. 2013. *Chem. Rev.* 113:9043–85
van Dishoeck EF, Kristensen LE, Benz AO, et al. 2011. *Publ. Astron. Soc. Pac.* 123:138–70
van Kempen TA, Hogerheijde MR, van Dishoeck EF, et al. 2016. *Astron. Astrophys.* 587:A17
van Kempen TA, Kristensen LE, Herczeg GJ, et al. 2010. *Astron. Astrophys.* 518:L121
van Kempen TA, van Dishoeck EF, Güsten R, et al. 2009. *Astron. Astrophys.* 501:633–46
Vázquez-Semadeni E, Colín P, Gómez GC, Ballesteros-Paredes J, Watson AW. 2010. *Ap. J.* 715:1302–17
Velusamy T, Langer WD, Marsh KA. 2007. *Ap. J. Lett.* 668:L159–62
Walawender J, Bally J, Kirk H, Johnstone D. 2005a. *Astron. J.* 130:1795–804
Walawender J, Bally J, Kirk H, et al. 2006. *Astron. J.* 132:467–77
Walawender J, Bally J, Reipurth B. 2005b. *Astron. J.* 129:2308–51
Wardle M, Koenigl A. 1993. *Ap. J.* 410:218–38
Waters LBFM, Waelkens C. 1998. *Annu. Rev. Astron. Astrophys.* 36:233–66
Weaver H, Williams DRW, Dieter NH, Lum WT. 1965. *Nature* 208:29–31
Williams JP, Plambeck RL, Heyer MH. 2003. *Ap. J.* 591:1025–33
Wilson RW, Jefferts KB, Penzias AA. 1970. *Ap. J. Lett.* 161:L43
Wiseman JJ, Ho PTP. 1996. *Nature* 382:139–41
Wolf-Chase GA, Barsony M, O'Linger J. 2000. *Astron. J.* 120:1467–78
Wu Y, Wei Y, Zhao M, et al. 2004. *Astron. Astrophys.* 426:503–15
Yıldız UA, Kristensen LE, van Dishoeck EF, et al. 2013. *Astron. Astrophys.* 556:A89
Yıldız UA, Kristensen LE, van Dishoeck EF, et al. 2015. *Astron. Astrophys.* 576:A109
Yu KC, Bally J, Devine D. 1997. *Ap. J. Lett.* 485:L45–48
Yu KC, Billawala Y, Bally J. 1999. *Astron. J.* 118:2940–61
Yu KC, Billawala Y, Smith MD, Bally J, Butner HM. 2000. *Astron. J.* 120:1974–2006

Zapata LA, Arce HG, Brassfield E, et al. 2014. *MNRAS* 441:3696–702
Zapata LA, Fernández-López M, Curiel S, Patel N, Rodríguez LF. 2013a. *Astron. J.* Submitted. arXiv:1305.4084
Zapata LA, Ho PTP, Rodríguez LF, et al. 2006. *Ap. J.* 653:398–408
Zapata LA, Ho PTP, Schilke P, et al. 2009a. *Ap. J.* 698:1422–28
Zapata LA, Lizano S, Rodríguez LF, et al. 2015. *Ap. J.* 798:131
Zapata LA, Loinard L, Schmid-Burgk J, et al. 2011. *Ap. J. Lett.* 726:L12
Zapata LA, Menten K, Reid M, Beuther H. 2009b. *Ap. J.* 691:332–41
Zapata LA, Rodríguez LF, Ho PTP, et al. 2005. *Ap. J. Lett.* 630:L85–88
Zapata LA, Rodríguez LF, Kurtz SE, O'Dell CR. 2004a. *Astron. J.* 127:2252–61
Zapata LA, Rodríguez LF, Kurtz SE, O'Dell CR, Ho PTP. 2004b. *Ap. J. Lett.* 610:L121–24
Zapata LA, Schmid-Burgk J, Ho PTP, Rodríguez LF, Menten KM. 2009c. *Ap. J. Lett.* 704:L45–48
Zapata LA, Schmid-Burgk J, Pérez-Goytia N, et al. 2013b. *Ap. J. Lett.* 765:L29
Zinnecker H, McCaughrean MJ, Rayner JT. 1998. *Nature* 394:862–65
Zinnecker H, Yorke HW. 2007. *Annu. Rev. Astron. Astrophys.* 45:481–563
Zuckerman B, Kuiper TBH, Rodriguez Kuiper EN. 1976. *Ap. J. Lett.* 209:L137–42
Zweibel EG, Hole KT, Mathieu RD. 2006. *Ap. J.* 649:879–87